UNITED NATIONS EDUCATIONAL, SCIENTIFIC AND CULTURAL ORGANIZATION
INTERNATIONAL ATOMIC ENERGY AGENCY
INTERNATIONAL CENTRE FOR THEORETICAL PHYSICS
I.C.T.P., P.O. BOX 586, 34100 TRIESTE, ITALY, CABLE: CENTRATOM TRIESTE

H4.SMR/916 - 23

SEVENTH COLLEGE ON BIOPHYSICS:

Structure and Function of Biopolymers: Experimental and Theoretical Techniques.

4 - 29 March 1996

Polar and Chiral Symmetry and Biological Function

Jaques PROST
Institut Curie
Section de Recherche
Paris, France

Polar and Chiral symmetry and biological function.

Prost Jacques
Institut Curie
Section de Recherche
11 rue Pet M Curie
75231 PARIS - Cedex 05

Relations between symmetry and function have been understood for a long time at a macroscopic level. Stone age already mastered polar symmetry and Archimedes screw was able to play with both pseudo-vectorial and chiral symmetry to produce genuine vectorial symmetry, ie: the fluid flow). After the discovery by Pasteur in 1848 of the spontaneous chiral symmetry breaking in sodium and ammonium

pasteurisate, it was soon recognized that the living organisms were able to recognize and select enantiomers (A.P. Dubrunfaut 1847 had observed the selecting of yeasts between different carbohydrates, but the real symmetry perspective was put forward by Pasteur in 1858). So there is a long and dense history of symmetry related phenomena in biology, and clearly in these few lectures it is not possible to review all aspects. Instead, I will chose two aspects, one related to polarity and one to chirality and polarity, and try to extract whatever general feature can be extracted in order to find out wether or not we can get novel ideas and understanding from the observation of mechanisms used by nature.

A) Molecular Motors:

The first example is concerned with "molecular motors". Cellular life is

extremely complex, as we know, and one of the most fascinating features of the cell activity is the remarkable directivity and accuracy of its transport system. Enzymes are directed in whatever compartment they should go, chemical signals using vesicles are carried unidirectionally using distances and at such speeds that simple diffusion can be totally discarded. In fact we know now that this transport is maintained by proteins called molecular motors which move along one dimensional structures called generically "cytoskeleton". A good comparism might be a train system: the engine would be the molecular motors, and the track would be the cytoskeleton. We can identify essentially two types of tracks: the actin and the tubulin filaments. Although they are significantly different from each other (Fig 1), they share in common two very important structural features.

Fig 1 : (Molecular biology of the cell. 3rd Edit).

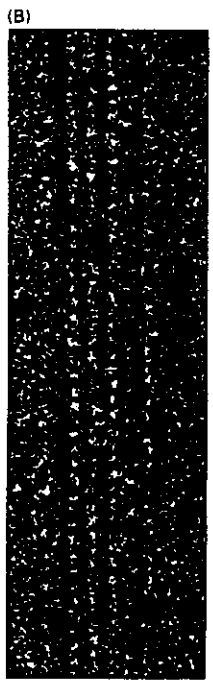

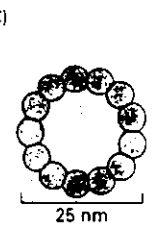

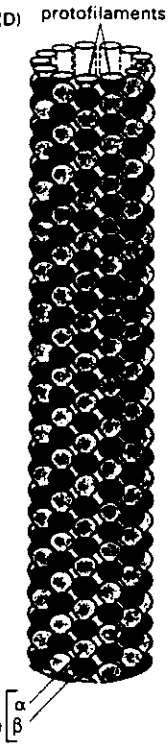

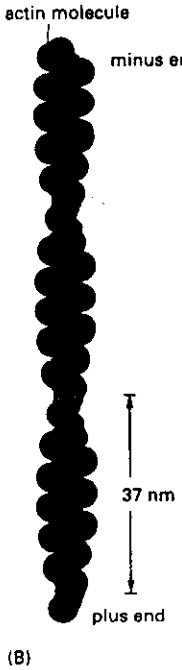

Figure 16–49 Actin filaments.
(A) Electron micrographs of negatively stained actin filaments. (B) The helical arrangement of actin molecules in an actin filament. (A, courtesy of Roger Craig.)

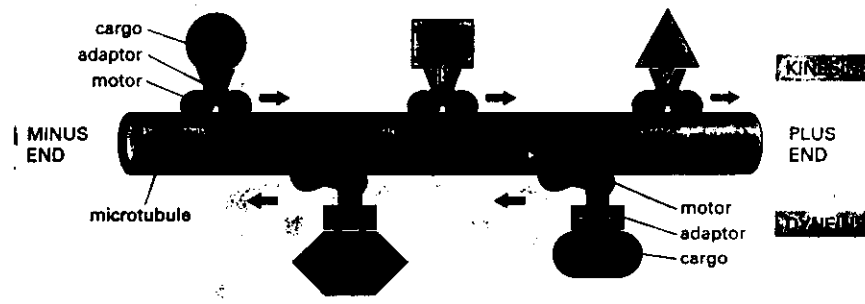

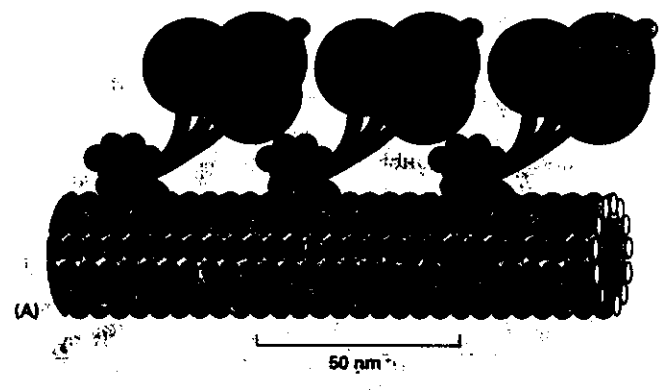

- they are one dimensional periodic structures
- they are polar.

Actin filaments can be "read" by myosin and tubulin filaments by kinesins or dyneins. These are in fact protein families which members are close to each other. It is believed that these proteins can exist in at least two states one being often referred to as the "rigor" state, and the other as the "free" state. The transition between the two states can in principle be easily triggered by thermal excitations, but it can also be activated by ATP by myosin's.

All these proteins can be purified and reconstituted in vitro allowing for well controlled experiments. They are essentially of two kinds: - motility assays, in which the motors adhere to a substrate from a non active part, and are randomly

Fig 2

Motility Assays.

a)

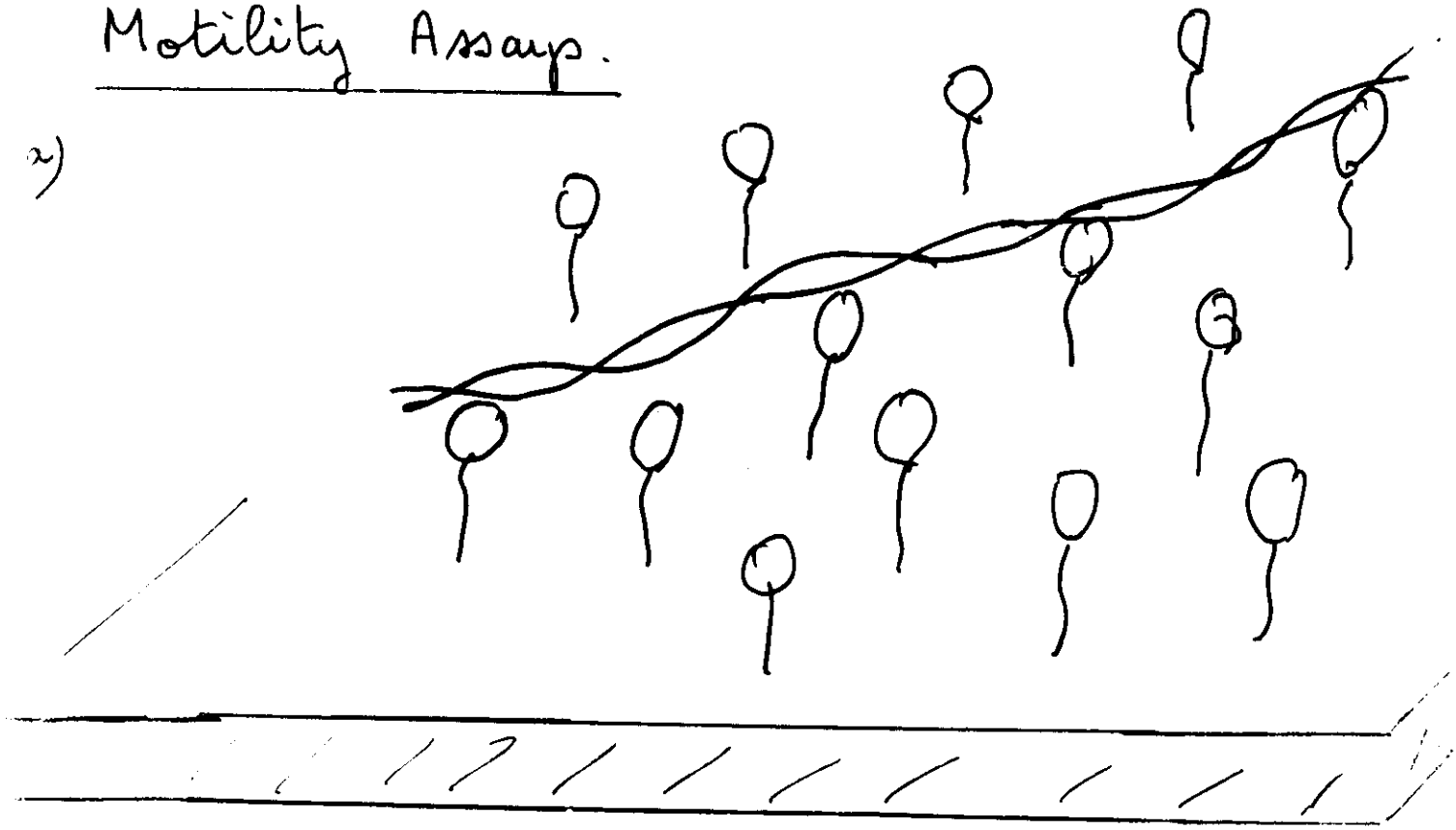

b) Actin - Myosin :

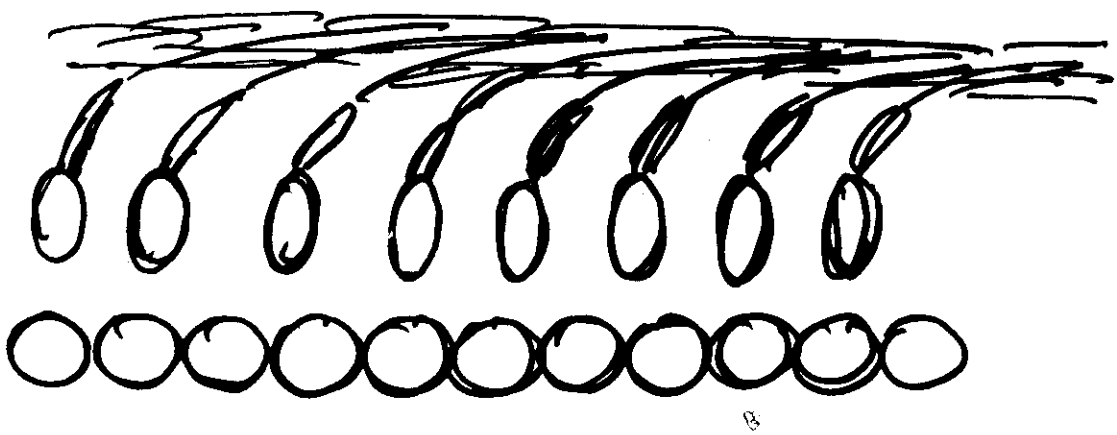

J. Spudich, 372, 515 (1994).

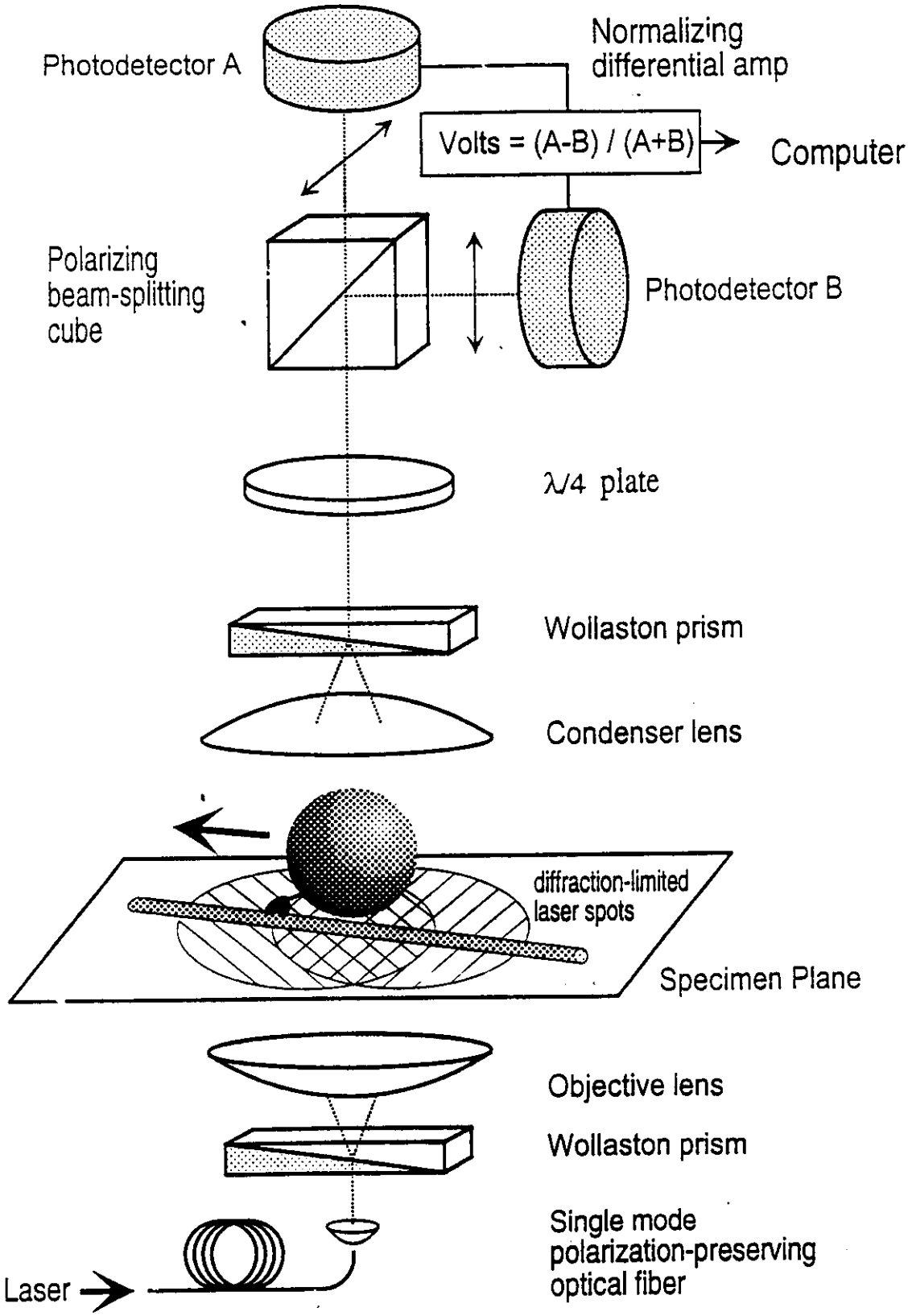

Svoboda & Block, Fig. 1

distributed on it (Fig 2a)

- single motor experiments (Fig 2).

In the first kind, filaments sedimented in the motor. In the absence of ATP, nothing happens. In the presence of ATP we can see the filaments moving unidirectionally. One can get good data relating the average velocity with the ATP concentration, and surface coverage. The second type of experiments, recently developed allows to follow the motion of a single motor: again, ATP consumption is required, and the analysis of the statistics of the motion shows that it is quantized with steps corresponding to the filament size (in the case of kinesin (Fig 4). The myosin steps seem to be more related to a conformational change. Actually, a third and very important motor/filament configuration should be mentioned: that found in muscles where myosin bundles move on the actin filaments in a [illegible] fashion. We will come back on that point later.

Fig 4 :

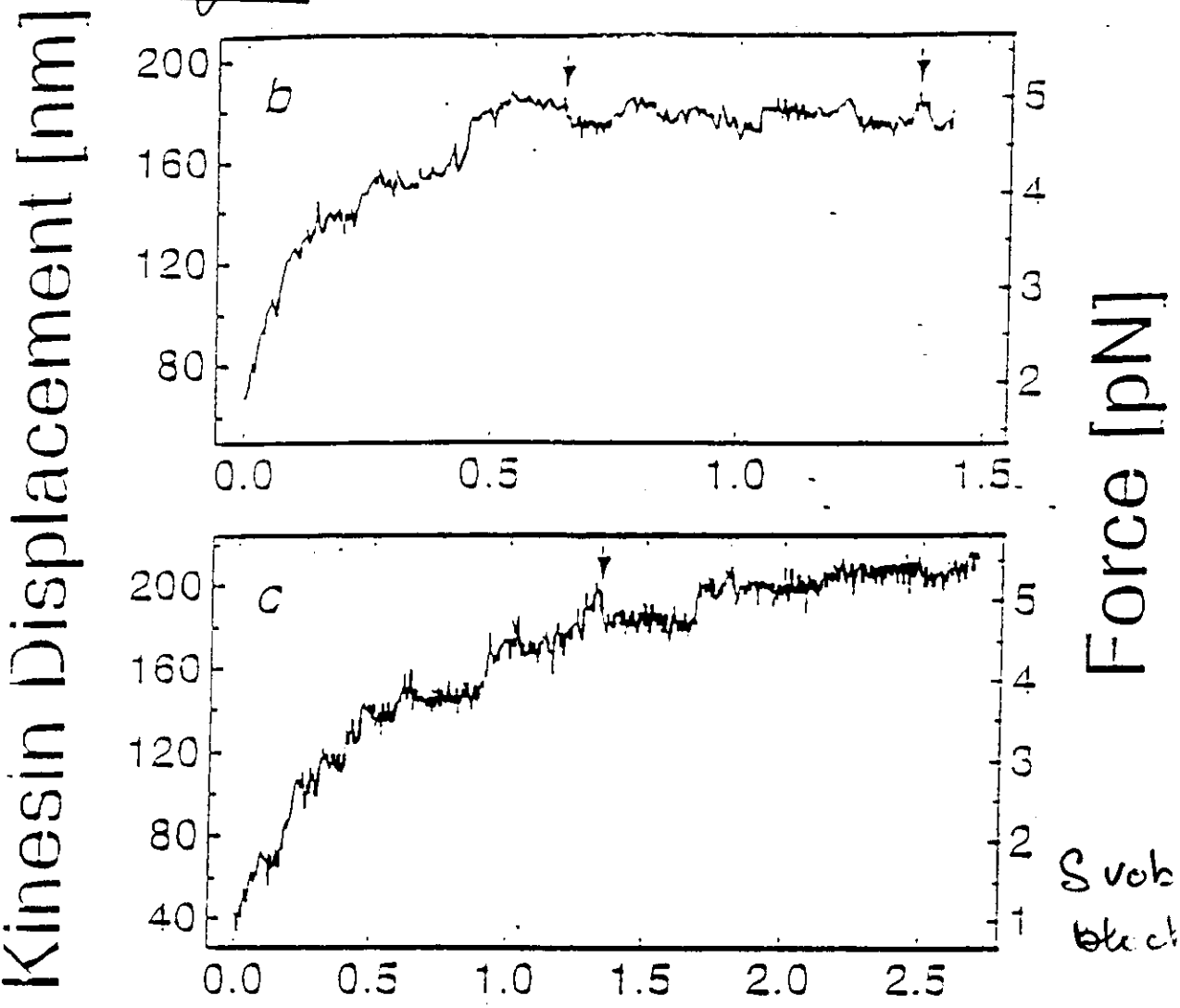

Svoboda and Block Nature

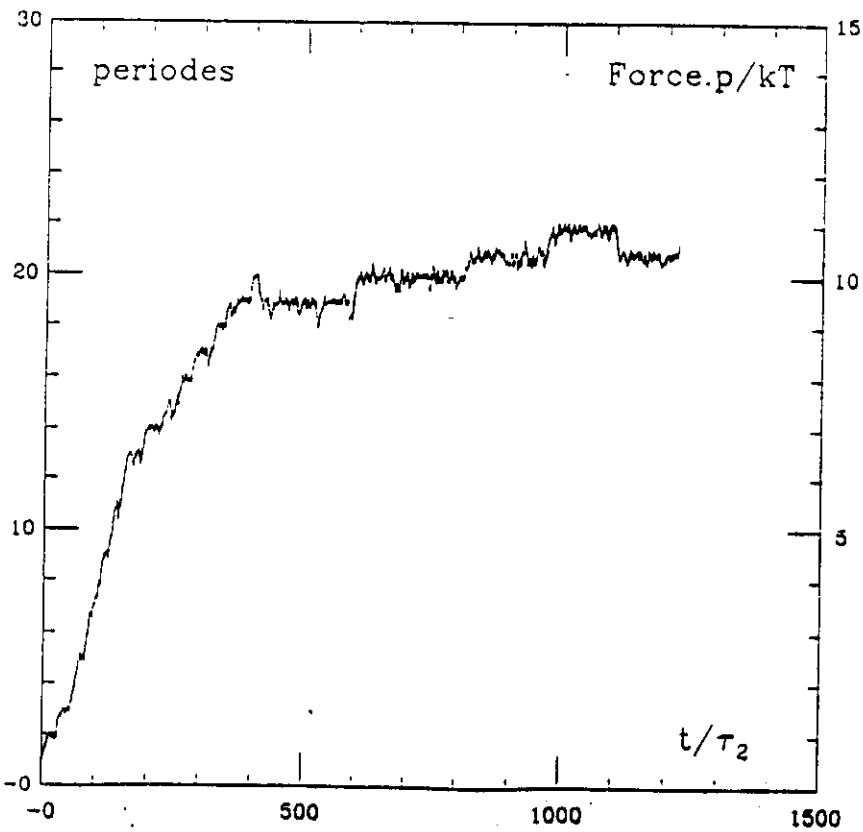

$\bar{w}_1 = 15$, $\bar{w}_2 = 5$

$\delta = 0.5$

$D_0 \tau_2 / \rho^2 = 10^{-2}$

$\frac{a}{a+b} = 10^{-1}$

1) Single Motors:

Can we understand this motion from a symmetry standpoint? At first, one could be tempted to think that polarity itself is enough to define a velocity since both quantities have polar symmetry. However, this is not; indeed suppose that we find a relation between the velocity and the filament direction: in the absence of dissipation this relation must also hold after changing the time t in its opposite, that is the motor should go both in a direction and its opposite at the same time, which is of course impossible. This statement is after all not so profound: we all know that an engine needs fuel to be able to work. But conversely, we know from Curie principle that a protein interacting with a polar cytoskeleton filament and dissipating energy via ATP consumption (or any other mean), thus breaking the $t, -t$ symmetry, must move. The real question is: how, and what makes the

system efficient?

In order to try and answer these questions let us build up a very simple model, which as we will see is already quite rich. Let us make only one assumption, corresponding to the current prejudice: proteins can exist in at least two states, which we will denote 1 and 2. As a result of its interaction with the cytoskeleton filament, the protein experience an attractive energy $W_i(x)$, which is a periodic function of the coordinate x identifying the location of the protein (x is center of gravity along the filament (the index i refers to the state in which the protein is at the time t of observation) (fig 5). The equations of motions describing the probability $C_i(x,t)$ of the motorprotein to be at point x, time t in state i, have the standard structure of Fokker Planck equations with a source term. They simply express that the local rate of change of this

Two-state model:

Une seule hypothèse !

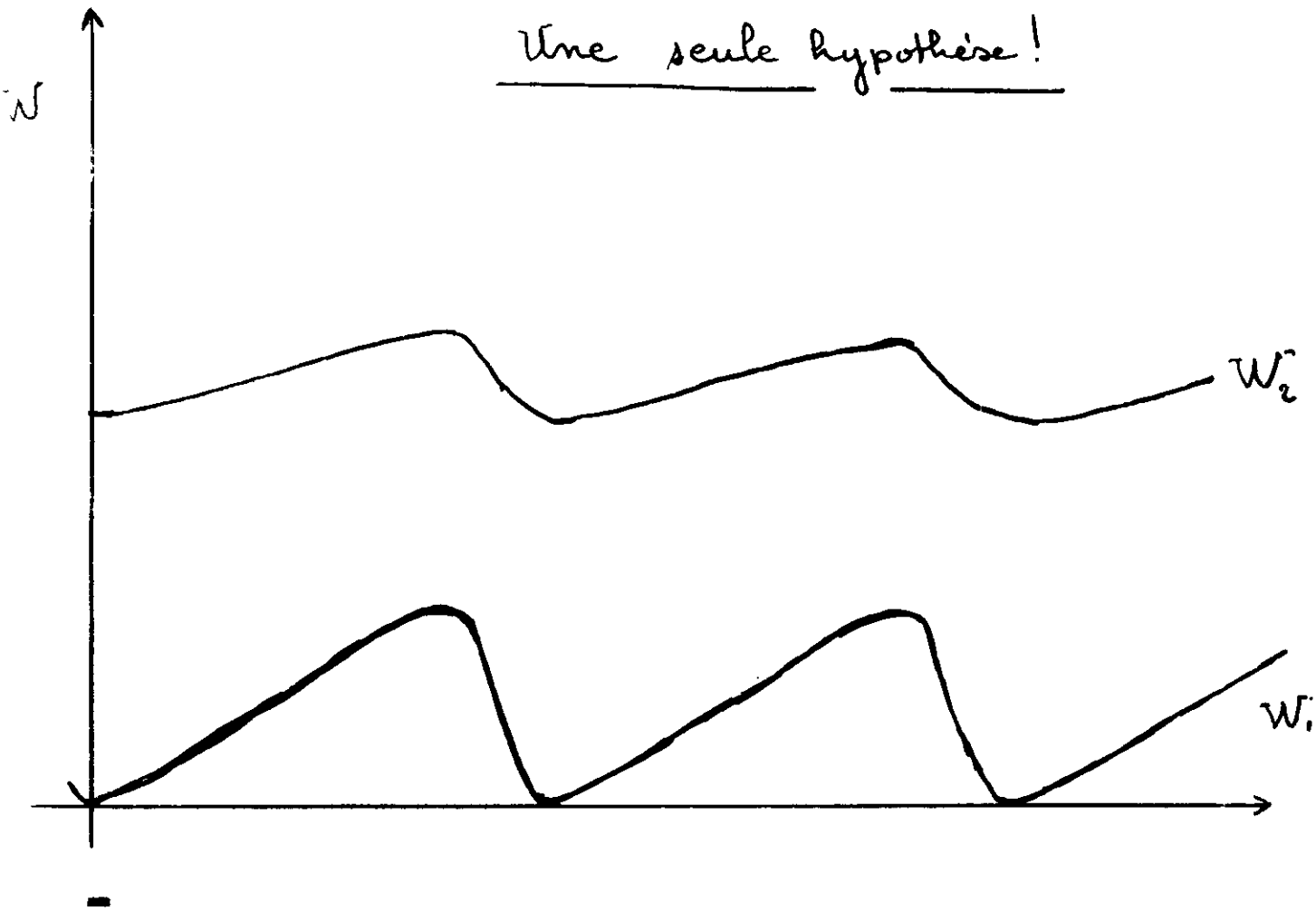

Fig 5

probability is due to what comes from the surfaces, the divergence term, and to the rate of change of one state into the other (the source terms).

$$\left.\begin{aligned} \frac{\partial c_1}{\partial t} + \operatorname{div} \vec{J}_1 &= -\omega_1 c_1 + \omega_2 c_2 \\ \frac{\partial c_2}{\partial t} + \operatorname{div} \vec{J}_2 &= \omega_1 c_1 - \omega_2 c_2 \end{aligned}\right\} \quad (1)$$

$$\left.\begin{aligned} J_1 &= -\mu_1 \left(c_1 \frac{dW_1}{dx} + kT \frac{dc_1}{dx} \right) \qquad \mu_1 = D_1 / kT \\ J_2 &= -\mu_2 \left(c_1 \frac{dW_2}{dx} + kT \frac{dc_2}{dx} \right) \qquad \mu_2 = D_2 / kT \end{aligned}\right\} \quad (2)$$

J_i is the protein fluxes in state i, μ_i is the mobility in state i, Einstein relation linking the mobility and diffusion constant in both states holds.

ω_1 is the transition rate from state one to state two, and ω_2 the reverse (ie $2 \to 1$).

In the absence of ATP consumption, detailed balance has to be satisfied:

$$\omega_1(x) \exp\left(-\frac{W_1(x)}{kT}\right) = \omega_2(x) \exp\left(-\frac{W_2(x)}{kT}\right) \quad (3)$$

The ATP consumption may be measured just by how much this reaction is broken:

$$\Omega = \omega_1 - \omega_2 \exp\left(\frac{W_1 - W_2}{kT}\right) \qquad (4)$$

Let us first show how the symmetry requirement has been exercised in the introduction ones in the average motion of a given protein is measured by the total flux $J = J_1 + J_2$ since it is the either of these two rates. It is straightforward to write, if $c = c_1 + c_2$, $c_1 = \lambda c$ $c_2 = (1-\lambda) c$:

$$J = -\mu_{eff}\left(c \frac{dW_{eff}}{dx} + \frac{dc}{dx}\right)$$

With

$$W_{eff}(x) - W_{eff}(0) = \int_0^x dx' \frac{\mu_1 \lambda \frac{dW_1}{dx} + \mu_2 (1-\lambda) \frac{dW_2}{dx}}{\mu_1 \lambda + \mu_2 (1-\lambda)}$$

$$+ kT \left[\ln \mu_{eff}\right]_0^x \qquad (5)$$

$$\mu_{eff} = \lambda \mu_1 + (1-\lambda) \mu_2$$

In steady state, λ is time independent and follows the potential symmetry. If the potentials are symmetrical, then the integrand is antisymmetrical, and the integral vanishes over one period p:

$$W_{eff}(p) = W_{eff}(0) \quad (= W_{eff}(np);\ n \text{ integer})$$

As a result the effective potential is essentially flat over a large number of periods (ie: no average slope), and no directed motion can result. We find here the necessity for asymmetry, a contrario. If detailed balance holds:

$$\lambda = \frac{\exp\left(-\frac{W_1}{k_B T}\right)}{\exp\left(-\frac{W_1}{k_B T}\right) + \exp\left(-\frac{W_2}{k_B T}\right)}$$

And (5) can be calculated exactly to give the free energy of the protein in interaction with the filament:

$$W_{eff}(x) - W_{eff}(0) = -kT \left[\ln\left(\exp\left(-\frac{W_1}{kT}\right) + \exp\left(-\frac{W_2}{kT}\right) \right) \right]_0^x$$

This is a periodic function, and again for any kind of potential, if the tracer is directed along the channel there will be no motion (only diffusion).

However, if W_1, W_2 have polar symmetry, if $\Omega \neq 0$, in general $W_{eff}(\rho)$ will be different from $W_{eff}(0)$. Thus, if we call $\delta W_{eff} = W_{eff}(\rho) - W_{eff}(0)$, the effective potential develops an average slope:

$$W_{eff}(n\rho) = n\, \delta W_{eff}, \text{ corresponding}$$

to the average force:

$$\overline{F_{eff}} = -\frac{\delta W_{eff}}{\rho}.$$

All of this does not tell us how efficient this process is. To get this insight one needs to solve equations

$\Omega(1), \Omega(2)$ with a specified potential shape. This can be done analytically with piecewise linear potentials, if thermal excitations can be neglected and with the further assumption ω_2 independent of space (Fig 6). I need under such circumstances the equations are piecewise linear, when either Ω is space independant, or $\Omega = \bar{\Omega}\,\delta(x-x_0)$ (ie Ω "strongly" localized). The last case corresponds to the notion of "active site" in biology: it tells us that the transition between state 1 and state 2, is basically impossible except when the motor protein has reached a particular location: the active site. The velocity versus excitation rate Ω that we can get differ fundamentally in these two cases (Figures 7 and 8). In the first one, the average velocity goes through a well defined maximum

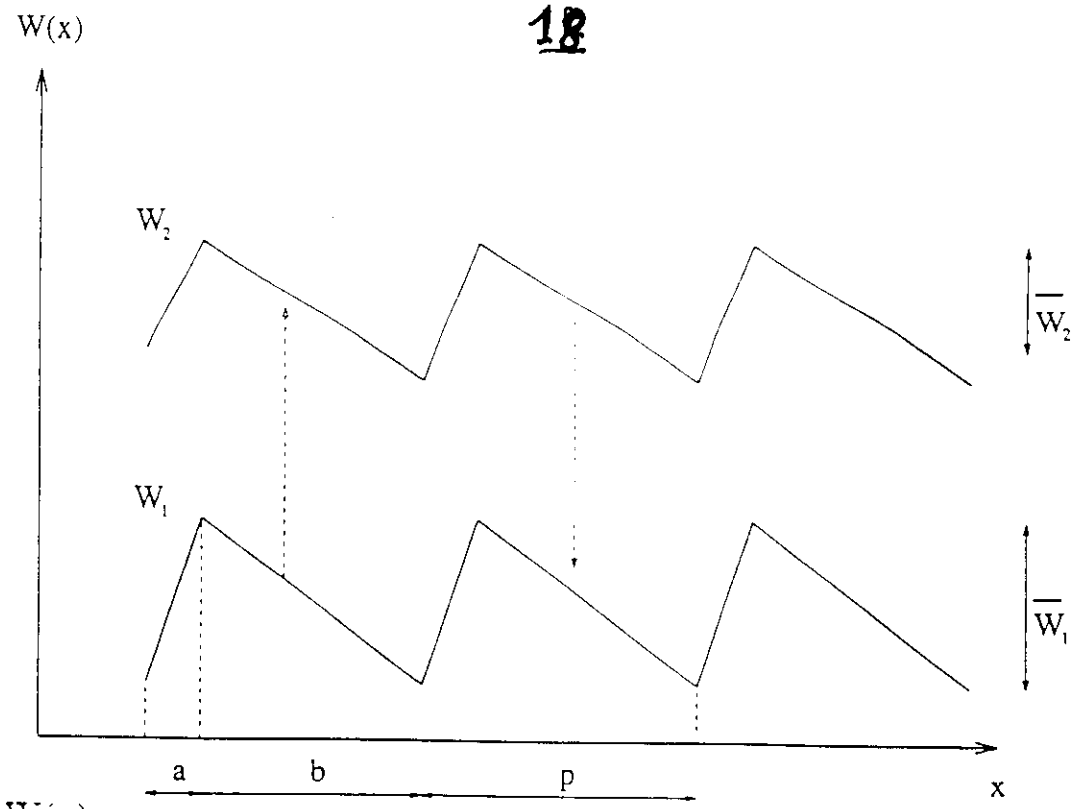

Fig 6.

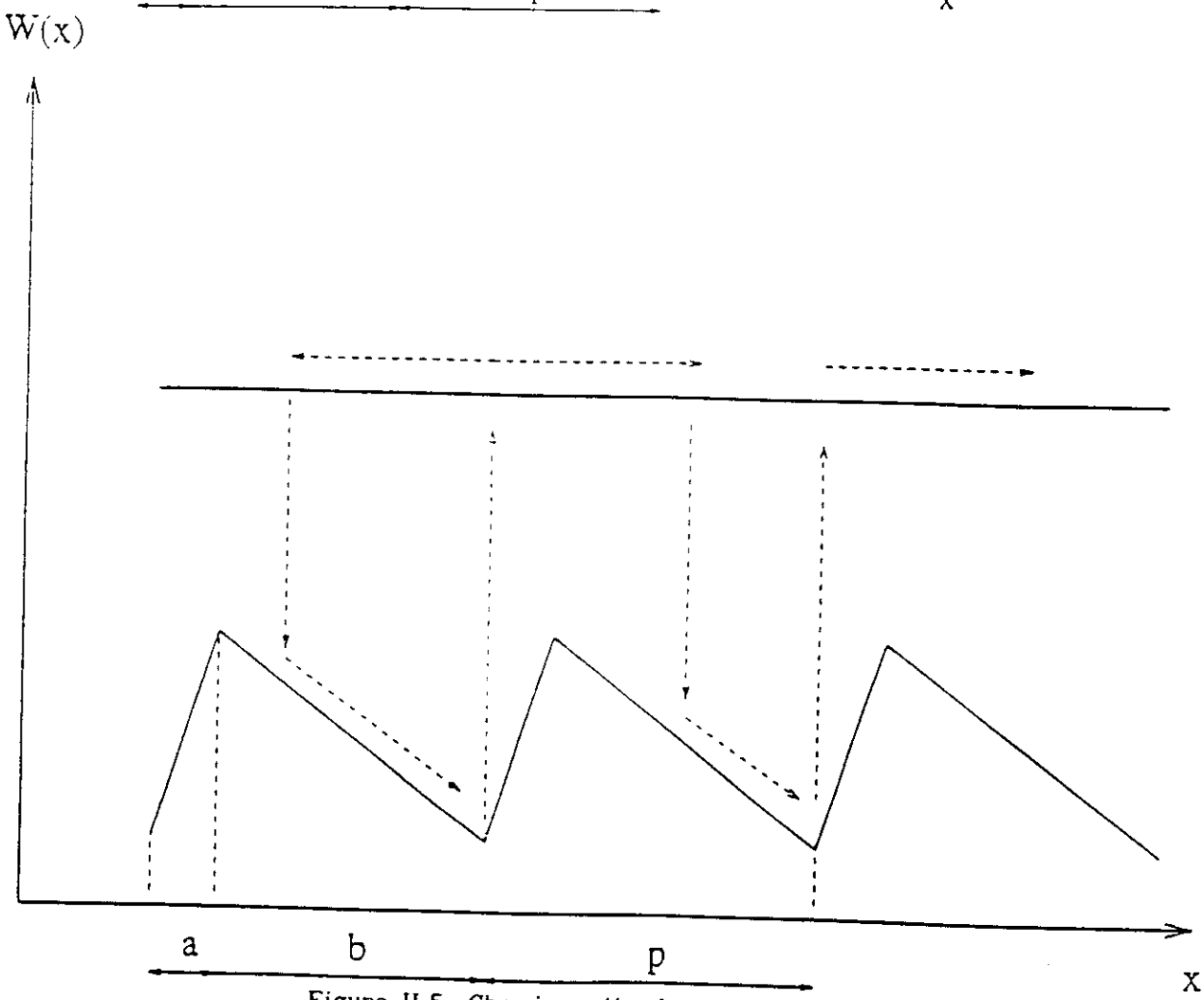

Figure II.5: *Chemin optimal suivi par les particules*

as Ω is increased, for any shape of the N_i's). At low excitation rate, the system is close to thermodynamical equilibrium and the velocity has to start from zero for $\Omega = 0$. Generically, it increases linearly with Ω. At large excitation rate, only the excited state is populated, and this restores a Boltzmann distribution in that state hence again the velocity vanishes like $1/(\Omega^3)$. The maximum velocity is obtained when twice, two characteristic times are matched (Fig 8); the case corresponding to a constant W_2 ("flat" excited state) is particularly simple to understand:

suppose we start from an excitation event from the energy minimum in the ground state to the excited state. After a typical lifetime $\tau_2 = \omega_2^{-1}$ in this excited state, the probability distribution of the motor protein is given by a gaussian curve of half width $\sqrt{2 D_2 \tau_2}$

$\Omega = cst$

$\frac{a}{a+b} = \frac{1}{10}$

$\overline{W}_1 = 10\ kT$

$\sqrt{D_0 \omega_2} = \frac{1}{\tau_2}\sqrt{D_0 \tau_2}$

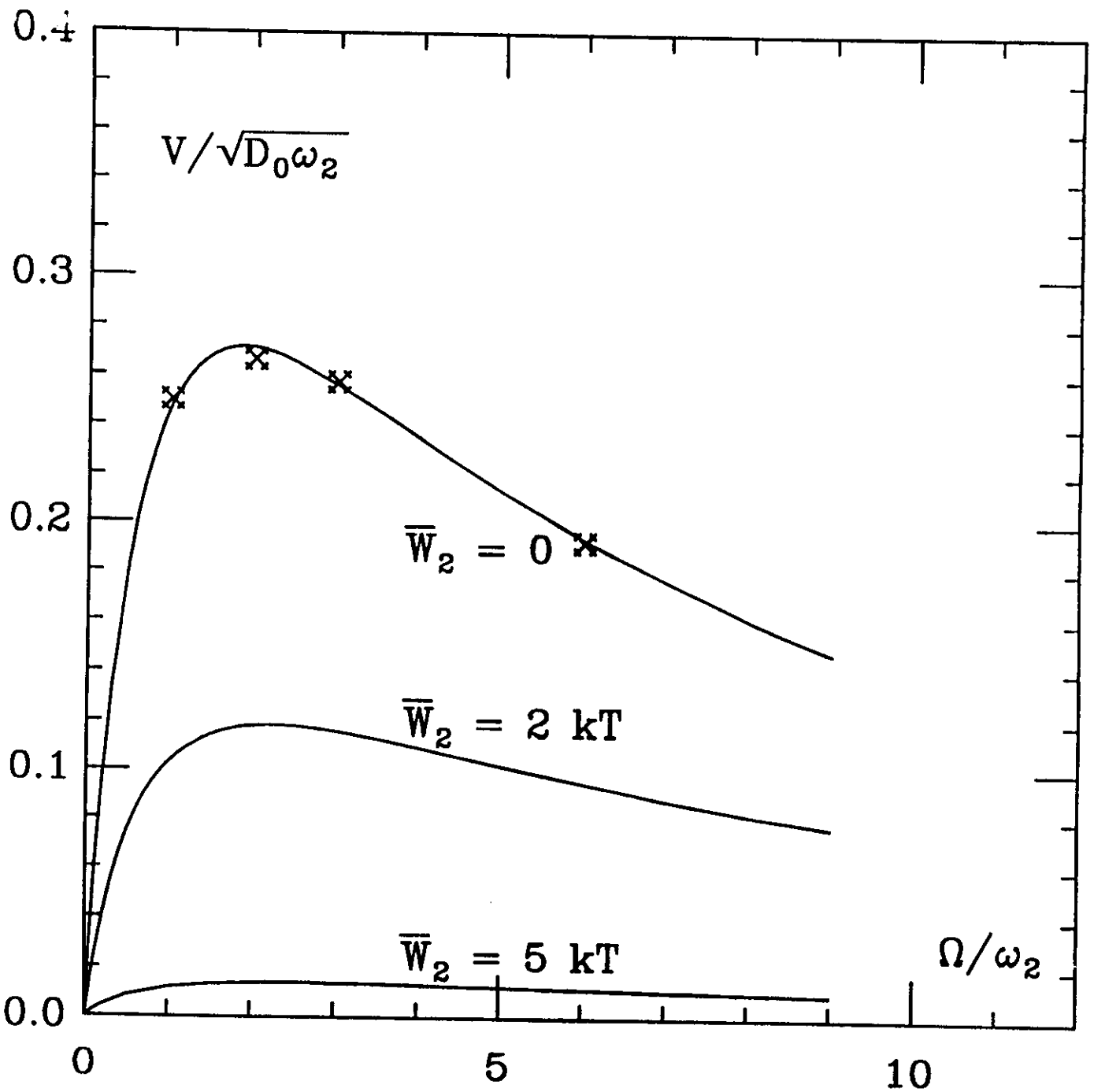

Fig 7

Localized excitation

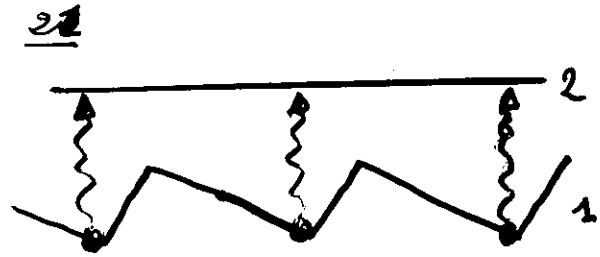

asymmetry $\frac{a}{a+b} = \frac{1}{10}$

$\overline{w_1} = 10\ kT$

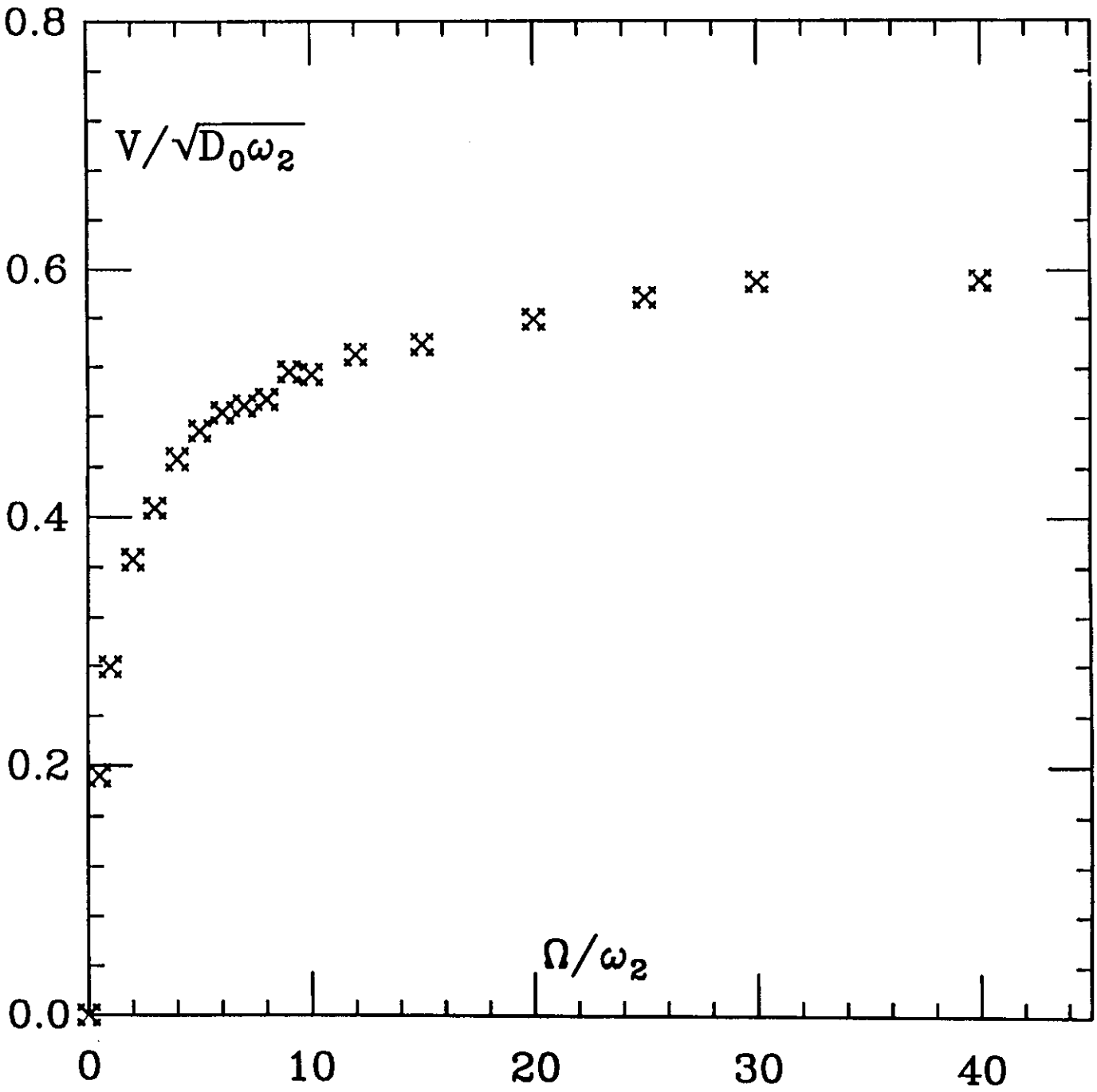

Fig 8

11)

$$\omega_1 = \omega_2 \exp\left(-\frac{W_2 - W_1}{kT}\right) + \Omega$$

Optimal Scenario

Fig 9

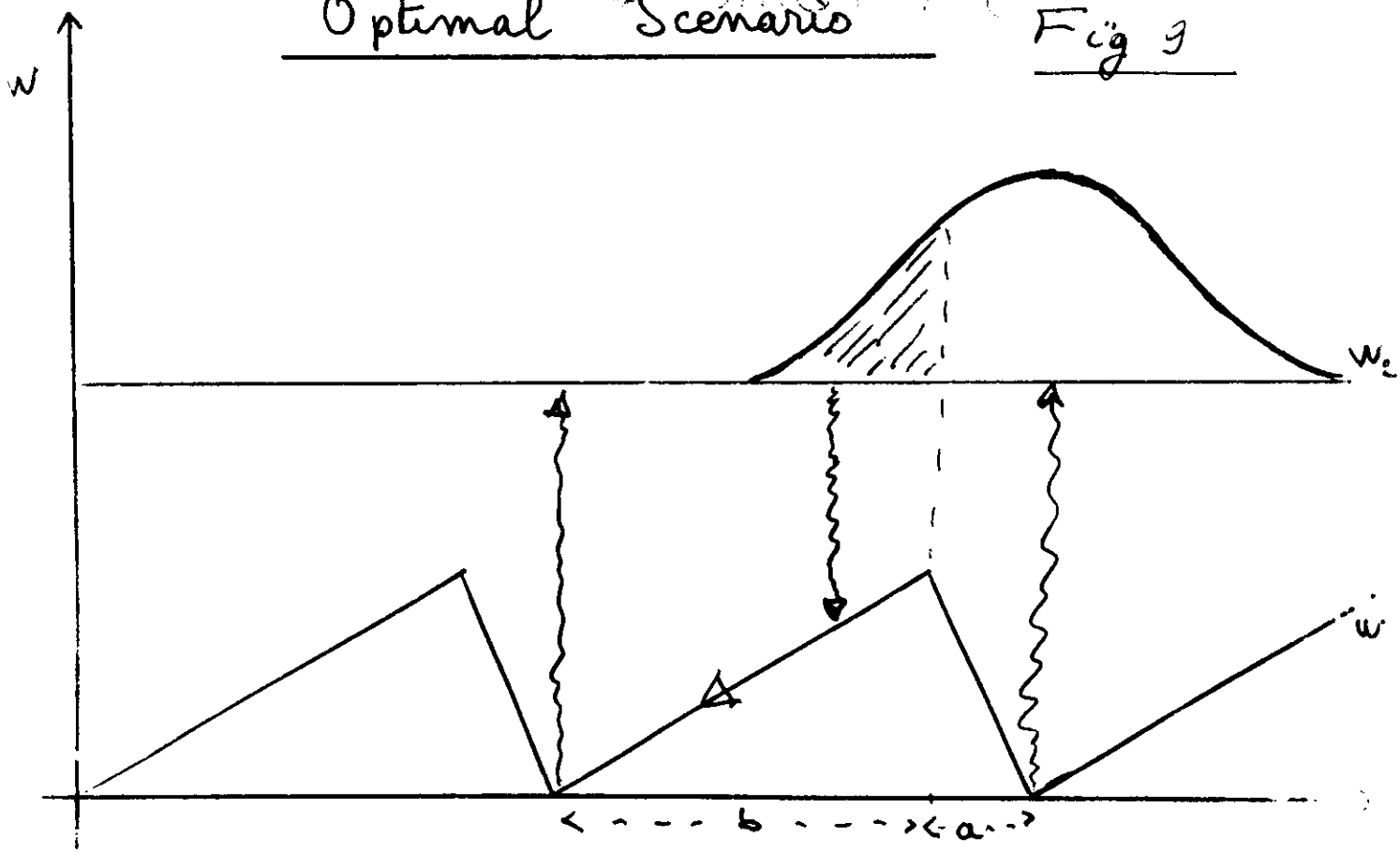

Homogeneous excitation: Match twice two times!

1) $a^2 \simeq 2 D_2 \tau_2 = 2 D_2 / \omega_2$

2) $\frac{1}{\Omega} \simeq \frac{b}{\left(\frac{D_1}{kT}\right)\left(\frac{W_1}{b}\right)}$ + $W_2 \simeq 0$

Localized case: only 1)

Biology: Svoboda et al, Nature (1993).
clearly localized Steps 80 Å
NO clustering (Kinosita)

$\bar{V} \simeq 0.5$ um/sec.

that part of the probability which is to the left of the ground state maximum (hatched part) will contribute to the motion, whereas that which is to the right will not. Once the protein is back in the ground state one wants it to move as far as possible, that is one wants the life time in the ground state to be comparable to the drift time along the long slope. This also tells us that the natural velocity scale is the diffusion distance in the excited state divided by the life time τ_2, that is

$$v_{typical} \simeq \sqrt{D_2 \omega_2}$$

If we take $D_2 \simeq 10^{-10}$ cm^2/sec $\tau_2 = \omega_2^{-1} \simeq 10^{-2}$ sec we get $v_{typical} \simeq \mu$m sec^{-1}. This is a reasonable order of magnitude, but of course it does not mean necessarily that the mechanism involves necessarily a diffusion step in real life!

When the excitation is highly localized,

there is no maximum in the $V(\Omega)$ curve: indeed, now the upper state can never be uniformly populated. A given protein is always excited from the energy minimum and contributes to the motion according to the gaussian partition. Since it will always slide downhill down to the energy minimum before being excited, the less time is spent in this minimum, the fastest is the cycle and the largest the velocity. So the maximum is pushed towards $\Omega = \infty$. Note that the relevant velocity is still the same, but that the absolute value is about twice longer in this latter case, everything else being kept alike.

The experimental curves show no evidence of a maximum when the velocity is plotted as a function of ATP concentration. This is in agreement with the idea of reactive sites used by biologists: only some pairing sites allow for the conformational change.

Note that we discussed here the two extremes $\Omega = \text{cte}$ and $\Omega = \bar{\Omega}\,\delta_n \pmod p$, but of course

in general Ω should be a smooth function of x. In fact for any non perfectly localized excitation rate there is a maximum at finite Ω. The comparison with experiment hence shows that localization is indeed really sharp.

In fact we have assumed that eventhough $W_1(x)$ and $W_2(x)$ have different shapes, their extrema did coincide. However this does not need to be true, furthermore the transition rates do not need to be local either in space x in time:

$$w_1 = w_1(x-x', t-t') \quad ; \quad w_2 = w_2(x-x', t-t')$$

or even more generally:

$$w_1 = w_1(x, x', t-t') \; ; \quad w_2 = w_2(x, x', t-t')$$

where x' is the location of the protein before the conformational change, x its location after, and the functions need to be periodic in both x and x'. Because of time translational invariance only the difference $t-t'$ can show up.

Let us first specialize to the simple case of fig 10. One clearly sees now that provided the life time in either

Fig 10.

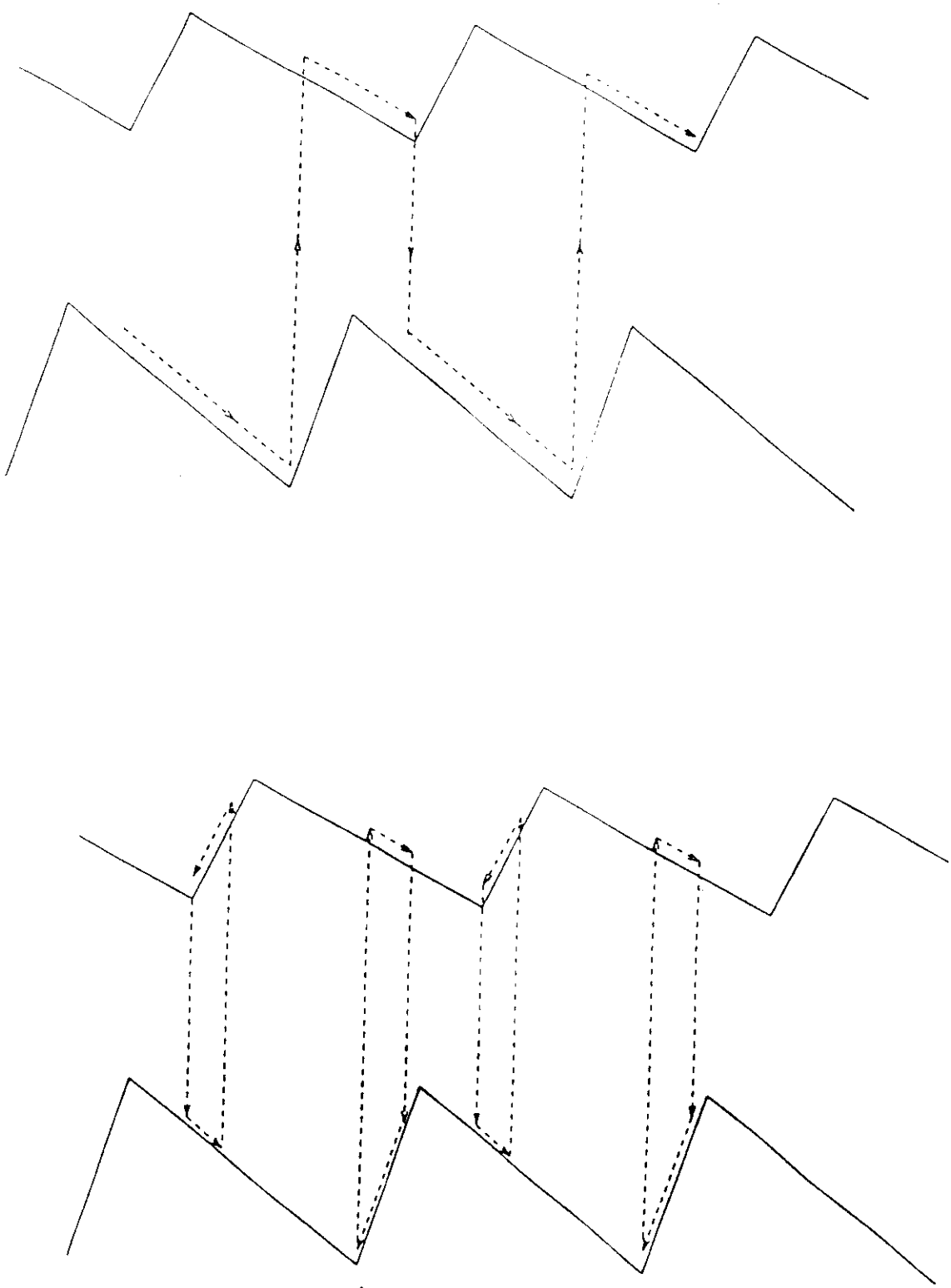

A

state is long enough or if excitation and deexcitation can only occur in the potential minima) a macroscopic motion will result easily from the out of equilibrium transitions between the two states. In fact what is more subtle to understand here, is why there is no motion when detailed balance is satisfied, but remember our general argument holds also in this case.

Now there is no diffusive step. The caracteristic velocity is

$V \simeq |\mu \nabla W|$ this can easily be ten times longer than the former estimate (see Fig 10) (i.e in the ratio W/kT) V. What we said about matching twice two time scales when $\Omega = cte$, was one if $\Omega = \bar{\alpha}\, \delta_0$ is still valid.

An other regime is worth being investigated: it corresponds to the case $W_2(x) = -W_1(x) + \text{const}$ (Fig 12). Clearly now, the direction of motion depends on time scale rather than on geometry. For the rest the features are essentially comparable to the former case.

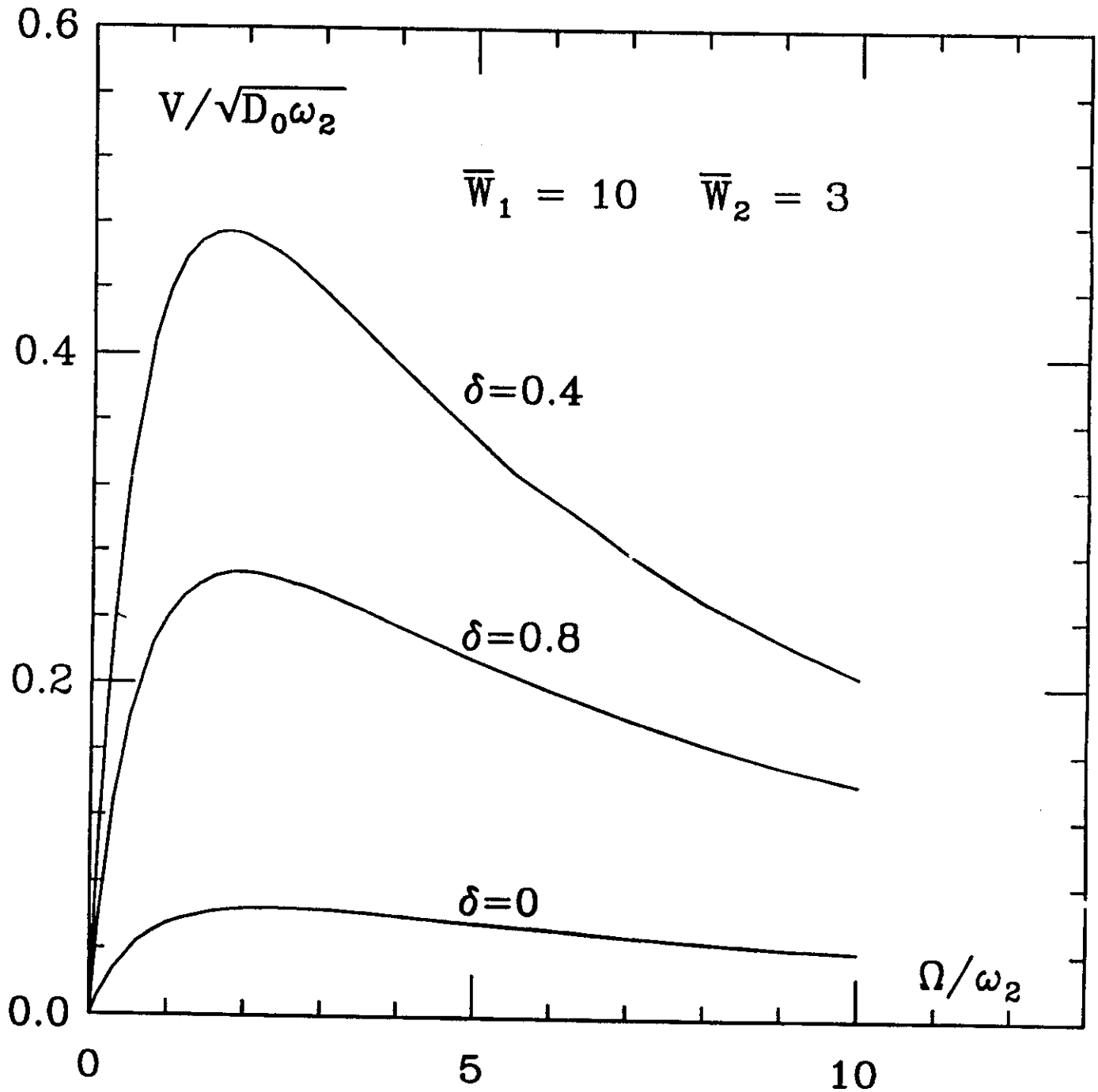
0.6
0.4
0.2
0.0
0
5
10
$V/\sqrt{D_0\omega_2}$
$\overline{W}_1 = 10 \quad \overline{W}_2 = 3$
$\delta=0.4$
$\delta=0.8$
$\delta=0$
Ω/ω_2

Fig 11

Velocity reversal.

R Doering, W. Horsthemke, J. Riordan Phys Rev Lett 72 (1994)
M. M. Millonas, M.I Dykman, Phys. Lett A 185 (1994).

$\tau_2 > \tau_1$

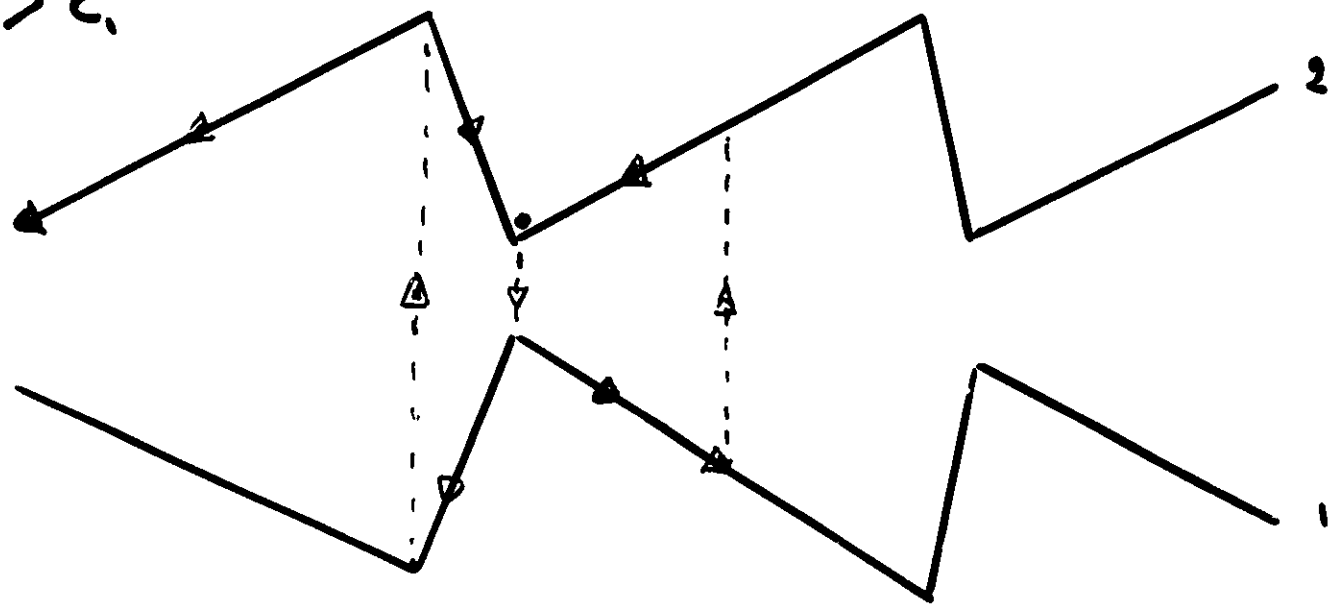

$\tau_1 > \tau_2$

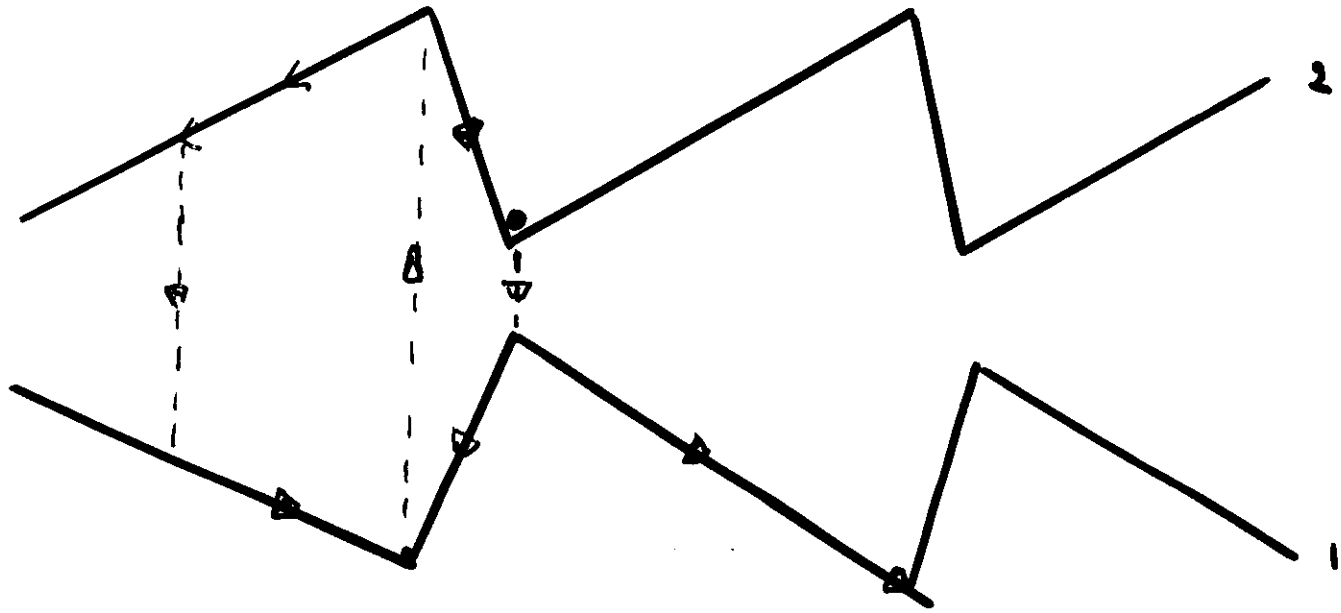

J. F Chauvin, A. Ajdari, J. Prost. Europhys. Lett (1995)

Separation ?

Fig 12

We have shown in Fig 14(b,c) two typical recordings of a displacement versus time of a kinesin on a tubulin filament. Since the motor moves against the optical trap, it gradually developps a force which opposes the motion and eventually stops it. The remarquable feature is the steps which can be seen and actually analyzed with appropriate statistical techniques: they correspond to the period 8 nanometers of the tubulin filaments. The bottom curve corresponds to a computer simulation with piecewise linear potentials like on figure 6: the similarity with experimental curves is striking but one could do as well with other sets of parameters, in particular with a diffusive step whereas this simulation corresponds to our type two (ie: "shifted potentials") escample.

Fig 13 a, b, c, again shows data extracted from Svoboda and Block ref: an essentially linear decrease of the velocity is observed as an opposing force is increased. Fig 14, 15 exhibit two theoretical curves each corresponding to a regime in which diffusion plays a role (Fig 14) (top curve, right: high ATP, bottom right: low ATP), and one in which the pinning

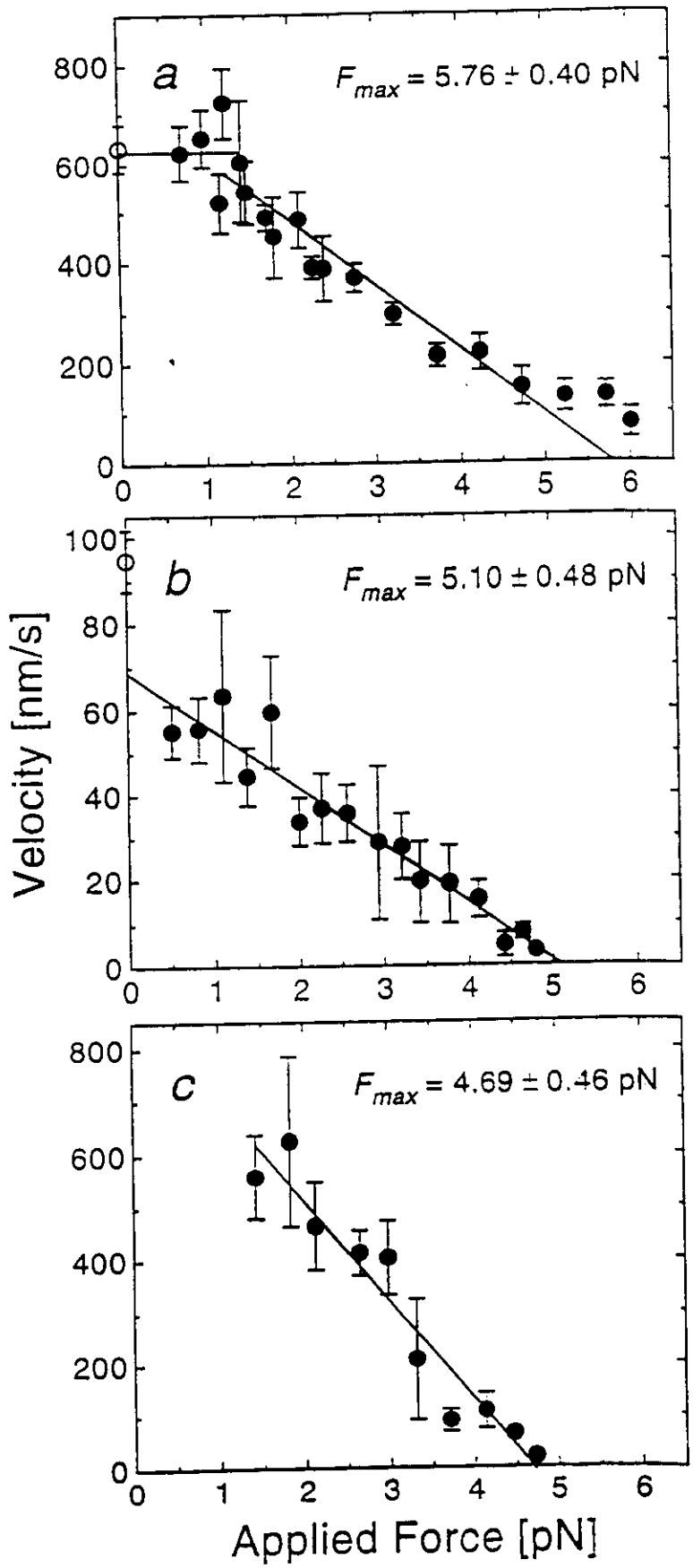

svobo la, fig. 9

Fig 13.

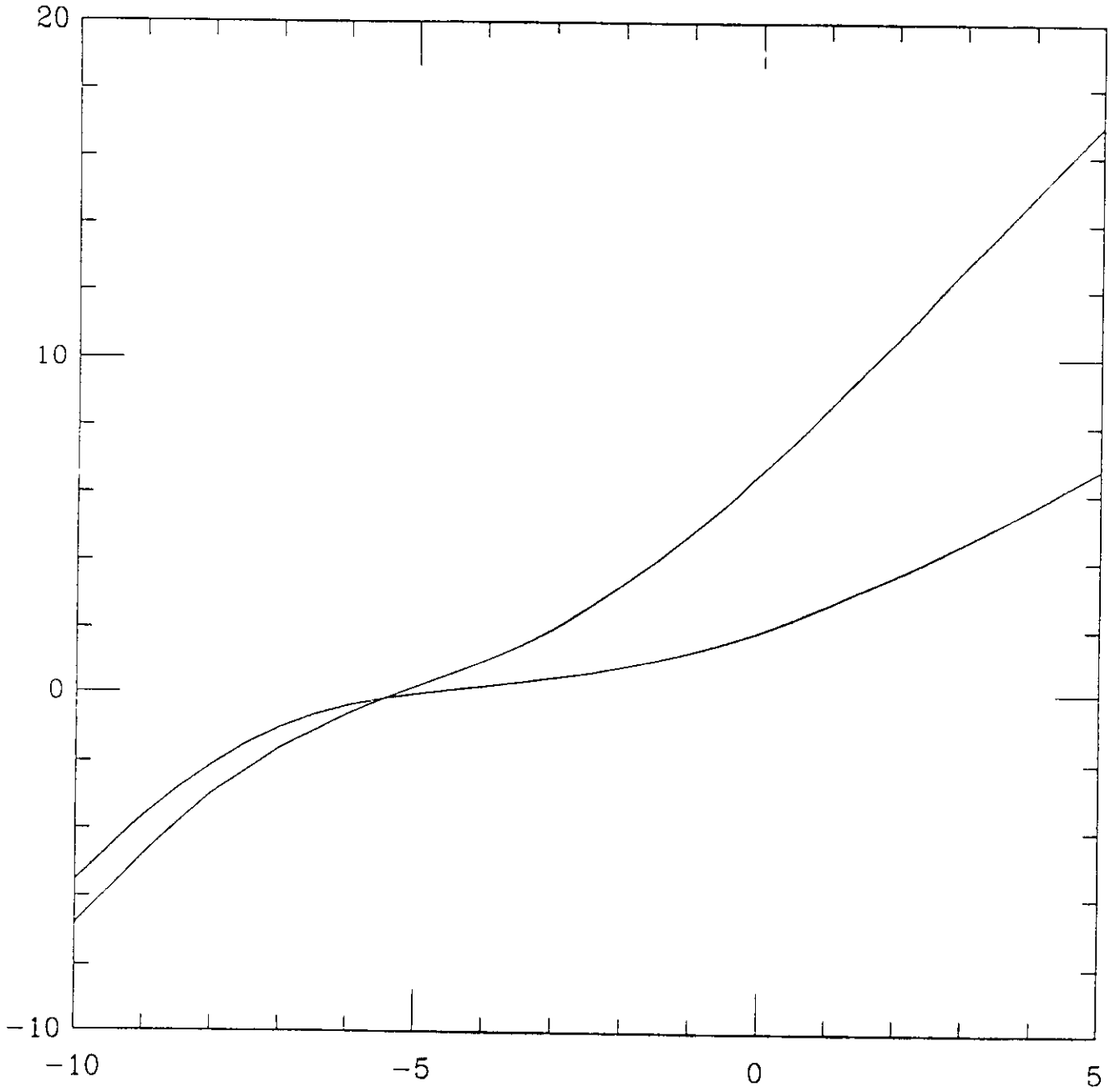

Fig 14

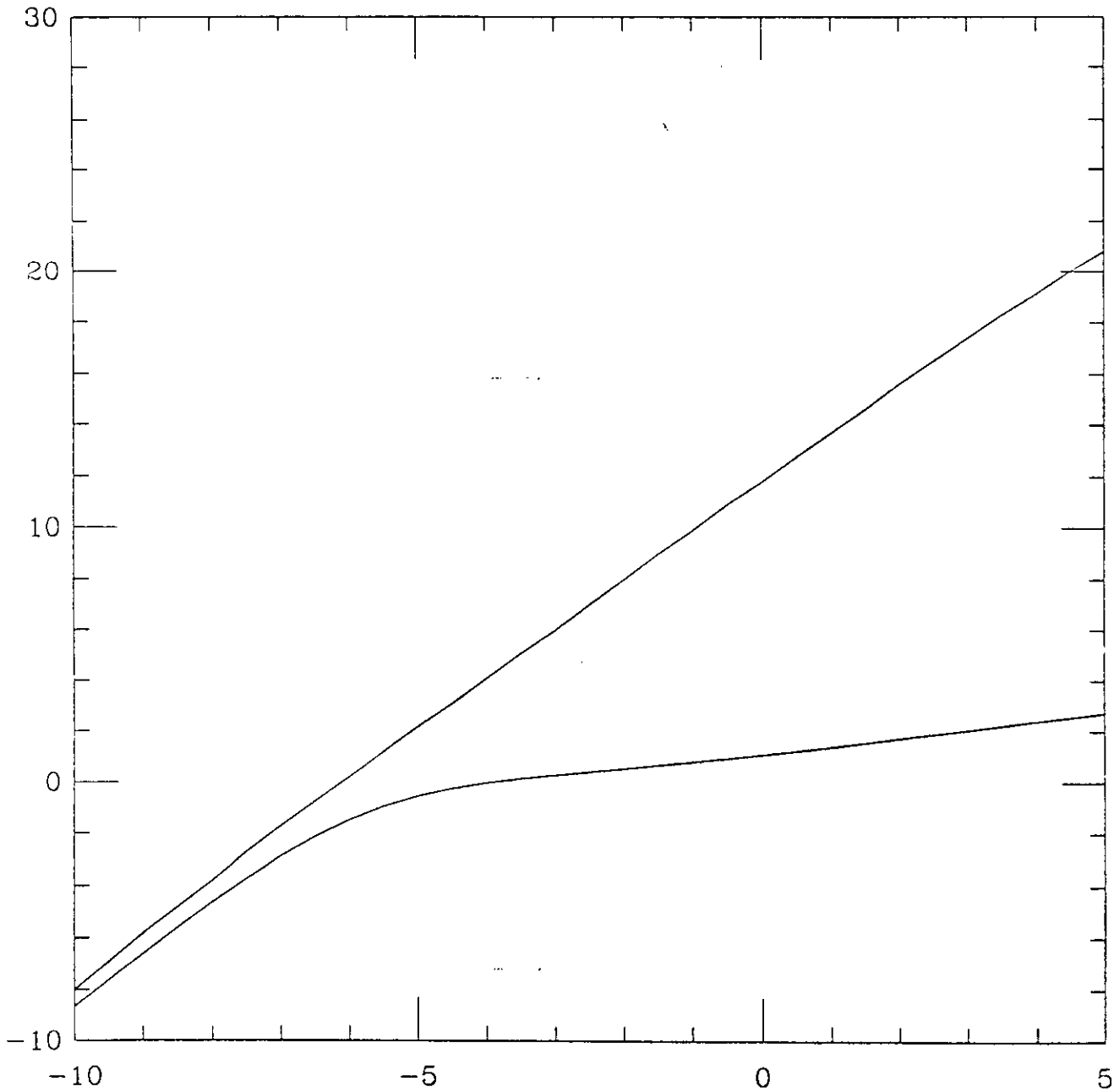

Fig 15.

potentials in each states are shifted with respect (Fig 15; top: high ATP, bottom low ATP)
to each other. Again it seems hard to decide which fits the data better especially in view of the fact that simply choosing "reasonable" parameters is enough to describe experimental datas. The one measurement which would be more decisive is that of the engine efficiency; we can define the efficiency as:

$$\Phi = \frac{\text{Work done per unit time}}{\text{[ATP] consumption per unit time, in energy units}}$$

$$\Phi = \frac{-f^{ext} \cdot V}{\Delta G \int_{-\infty}^{+\infty} \omega_i(x)\, c_i(x)\, dx}$$

Note that if we could have experimental data in which the force helps the motion we would be able to make the difference.

where ΔG is the [ATP] hydrolysis enthalpy, and $\int_{-\infty}^{+\infty} c_i(x)\,dx$ is normalized to one. A typical curve of Φ versus the external force is given on figure 15: it starts from zero for zero force, goes through a maximum and vanishes again with the velocity at the so called stall force. Assuming $\Delta G \simeq 13$ to $14\ kT$, one naturally gets efficiencies of several percents in the "diffusion regime" and much higher values up to thirty to forty percent in the shifted potential case (provided

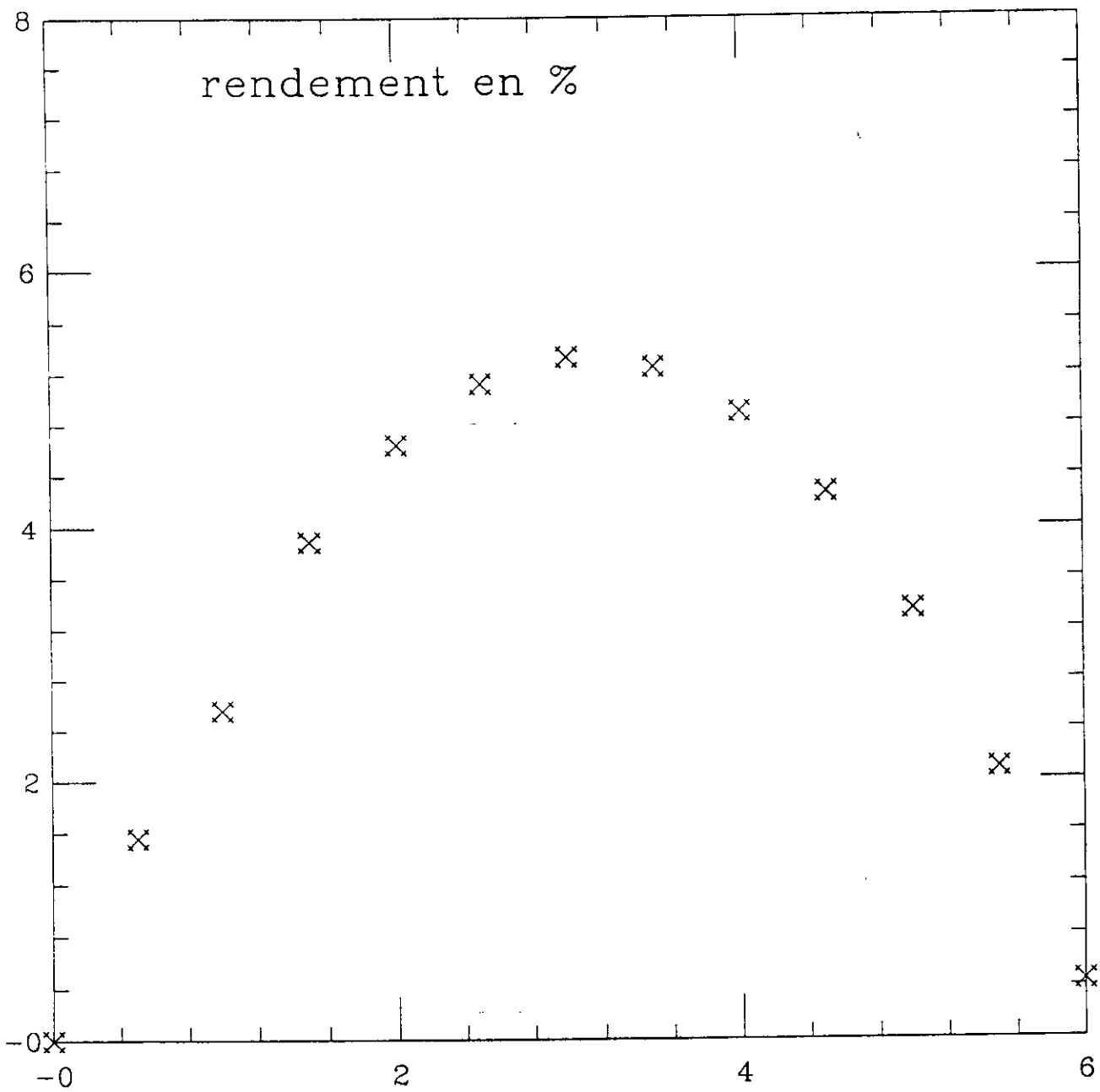

Fig 16

W_1 and W_2 are large compared to kT).

Note that the most popular model for myosins, a generalization of which is sketched on fig 17, is not fundamentally **different** from the ship-ratchet potential regime. We again expect a $V(\Omega)$ curve like the one of figure 8. Note also that regimes relevant for myosin need not be appropriate for kinesins & dyneins.

To sum up, what did we learn? First, we learned that for single motors both space and time symmetry breaking were essential. Second, that for motors to be efficients one needs to adjust times: this has nothing to do with the lock and key mechanism (note that the kind of selectivity we discuss must be appropriate for ion pumps as well). Third, that the absence of maximum in the velocity versus **excitation** rate curve confirms the idea of active sites developped by biologists.

The simple Ising like model that we **discuss** here, clearly can work in many different regimes which are basically all

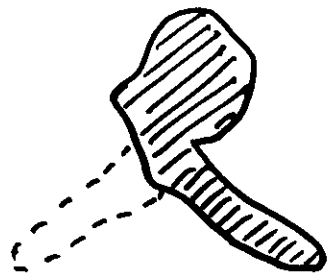

Huxley H.E.
(1966).

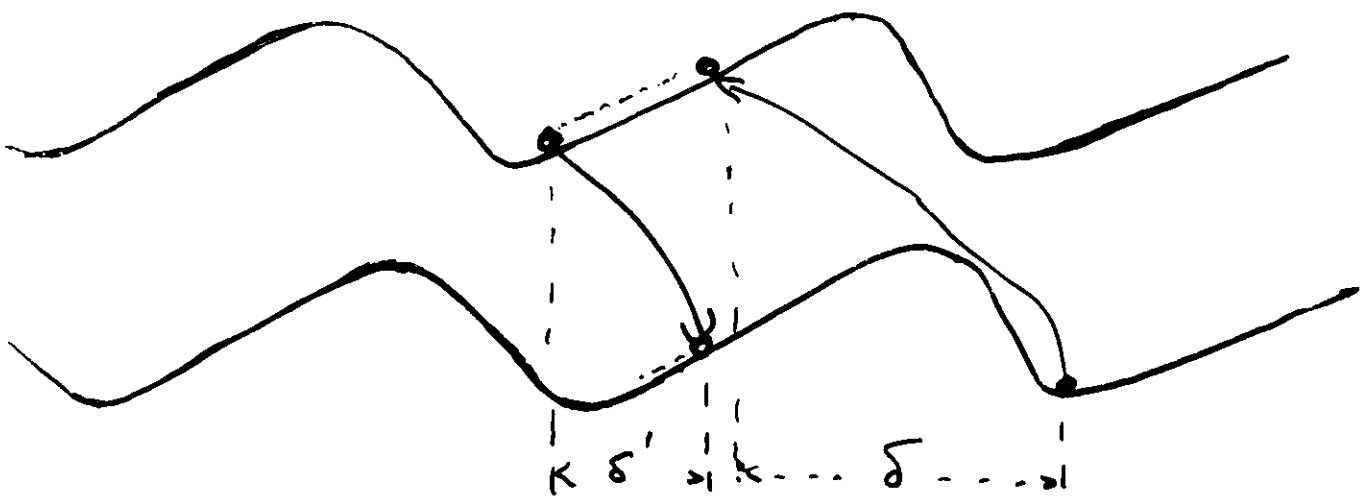

Fig 17

compatible with current experimental datas.

If we believe that we understand part of the physics which is involved in the motion of molecular motors, one should be able to construct artificial structures which mimic their essential features. This is what is shown in the following preprint, where we have designed polar and periodic structures which are able to exert pinning potentials $W_1(x)$ and $W_2(x)$ by a suitable addressing procedure, on colloidal particles in the 600 nanometer to several microns range. The preprint shows the basic principles of the experiment. The different regimes derived above are currently investigated at Princeton.

pre-solar grains with large ^{16}O enrichments. The Group 3 grains are ^{16}O-rich, but not with respect to both ^{17}O and ^{18}O. The discovery that ^{16}O can undergo mass-independent gas-phase chemical fractionation from both ^{17}O and ^{18}O has provided an alternative explanation for the observed ^{16}O enrichments in Solar System material[30].

Finally, if the Si/Al ratio is assumed to be solar in all stars and if all Al goes into corundum (Al_2O_3), interstellar corundum appears to be underabundant in meteorites, relative to interstellar SiC, by about a factor of between 20 and 50 (refs 4, 6, 10) when compaerd to estimated Galactic dust production rates[7,9]. This is in spite of the fact that, in the solar nebula, corundum should have been more stable than SiC. Possible explanations are that interstellar corundum has a finer grain size distribution than SiC and was thus not detected by our technique, that Al primarily condenses in other phases (such as silicates) that are less resistant to the chemical treatments used to isolate the grains or, most speculatively, that corundum has a shorter lifetime in the interstellar medium than SiC. □

Received 25 February; accepted 28 June 1994.

1. Anders, E. & Zinner, E. K. *Meteoritics* **28,** 490–514 (1993).
2. Ott, U. *Nature* **364,** 25–33 (1993).
3. Huss, G. R., Hutcheon, I. D., Wasserburg, G. J. & Stone, J. *Lunar planet. Sci.* **XXIII,** 563–564 (1992).
4. Nittler, L. R., Walker, R. M., Zinner, E. K., Hoppe, P. & Lewis, R. S. *Lunar planet. Sci.* **XXIV,** 1087–1088 (1993).
5. Huss, G. R., Hutcheon, I. D., Fahey, A. J. & Wasserburg, G. J. *Meteoritics* **28,** 369–370 (1993).
6. Hutcheon, I. D., Huss, G. R., Fahey, A. J. & Wasserburg, G. J. *Astrophys. J.* **425,** L97–L100 (1994).
7. Huss, G. R., Fahey, A. J., Gallino, R. & Wasserburg, G. J. *Astrophys. J.* (in the press).
8. Gehrz, R. D. in *Interstellar Dust* (eds Allamandola, L. J. & Tielens, A. G. G. M.) 445–453 (Kluwer Academic, Dordrecht, 1989).
9. Whittet, D. C. B. *Dust in the Galactic Environment*, 295 (Institute of Physics, Bristol, 1992).
10. Nittler, L. R., Alexander, C. M. O'D., Gao, X., Walker, R. M. & Zinner, E. K. *Lunar planet. Sci.* **XXV,** 1005–1006 (1994).
11. Gao, X., Alexander, C. M. O'D., Swan, P. D. & Walker, R. M. *Lunar planet. Sci.* **XXV,** 401–402 (1994).
12. Zinner, E. K., Tang, M. & Anders, E. *Geochim. cosmochim. Acta* **53,** 3273–3290 (1989).
13. Harris, M. J. & Lambert, D. L. *Astrophys. J.* **285,** 674–682 (1984).
14. Smith, V. V. & Lambert, D. L. *Astrophys. J. Suppl. Ser.* **72,** 387–416 (1990).
15. Iben, I. Jr. *Astrophys. J. Suppl. Ser.* **76,** 55–114 (1991).
16. Dearborn, D. S. P. *Phys. Rep.* **210,** 367–382 (1992).
17. Boothroyd, A. I., Sackmann, I. J. & Wasserburg, G. J. *Astrophys. J.* (in the press).
18. El Eid, M. F. *Astr. Astrophys.* **285,** 915–928 (1994).
19. Edvardsson, B. *et al. Astr. Astrophys.* **275,** 101–152 (1993).
20. Harris, M. J., Lambert, D. L., Hinkle, K. H., Gustafsson, B. & Eriksson, K. *Astrophys. J.* **316,** 294–304 (1987).
21. Kahane, C., Cernicharo, J., Gomez-Gonzalez, J. & Guelin, M. *Astr. Astrophys.* **256,** 235–250 (1992).
22. Forestini, M., Paulus, G. & Arnould, M. *Astr. Astrophys.* **252,** 597–604 (1991).
23. Gallino, R., Raiteri, C. M., Busso, M. & Matteucci, F. *Astrophys. J.* (in the press).
24. Nørgaard, H. *Astrophys. J.* **236,** 895–898 (1980).
25. Cameron, A. G. W. in *Protostars and Planets III* (eds Levy, E. H. & Lunine, J. I.) 47–73 (Univ. Arizona Press, 1993).
26. Prantzos, N., Doom, C., Arnould, M. & de Loore, C. *Astrophys. J.* **304,** 695–712 (1986).
27. Woosley, S. E. in *Nucleosynthesis and Chemical Evolution* (eds Hauck, B., Maeder, A. & Meynet, G.) 1–195 (Observatoire de Geneve, Geneva, 1986).
28. Clayton, R. N., Grossman, L. & Mayeda, T. K. *Science* **182,** 485–488 (1973).
29. Virag, A., Zinner, E. K., Amari, S. & Anders, E. *Geochim. Cosmochim. Acta* **55,** 2045–2062 (1991).
30. Thiemens, M. H. & Heidenreich, J. E. *Science* **219,** 1073–1075 (1983).
31. Renzini, A. & Voli, M. *Astr. Astrophys.* **94,** 175–193 (1981).
32. Lattimer, J. M., Schramm, D. N. & Grossman, L. *Astrophys. J.* **219,** 230–249 (1978).

ACKNOWLEDGEMENTS. We thank G. Huss and A. G. W. Cameron for their constructive reviews. This work was supported by NASA.

Directional motion of brownian particles induced by a periodic asymmetric potential

Juliette Rousselet*, Laurence Salome*, Armand Ajdari† & Jacques Prost†

* Centre de Recherche Paul Pascal, Avenue A. Schweitzer, 33600 Pessac, France
† Groupe de Physico Chimie Théorique, URA 1382 CNRS, E.S.P.C.I., 10, rue Vauquelin, 75231 Paris Cédex 05, France

STRUCTURES possessing spatial asymmetry should act as pumps in the presence of dissipation alone[1–4], without the need for macroscopic forces or temperature differences[5] to drive vectorial motion. It has been shown theoretically[2–4,6,7] that particles subjected to an asymmetric periodic potential can display net directional motion even if the space-averaged force is zero. Here we demonstrate such behaviour experimentally. We have studied the behaviour of colloidal particles suspended in solution and exposed to a sawtooth dielectric potential which is turned on and off periodically. The particles exhibit net motion with a velocity that depends on their size, suggesting applications in separation processes for objects in the size range 0.1–5 μm—a range that includes biological structures such as viruses, cells and chromosomes[8]. We furthermore point out the analogy between our device and motor protein assemblies.

Consider an asymmetric potential U_{on} applied periodically for a period τ_{on} and then switched off for a period τ_{off} (Fig. 1*A*). At the end of an 'on' period, the particles are trapped in the minima of the potential U_{on}, so that the concentration of particles is peaked around the corresponding positions (Fig. 1*B*). During the following 'off' period the particles diffuse freely so that the concentration at the end of this 'off' period is a set of gaussian curves centred around the same points (Fig. 1*C*). Turning the potential on again will induce 'downhill' motion of particles (Fig. 1*A*). The result of this off-on cycle is that the particles corresponding to the hatched areas move to the right, whereas essentially none move to the left. In a more general picture a proportion $P(m)$ would make an m-step progression, with $P(m) > P(-m)$ owing to the asymmetry. The result is to achieve macroscopic drift in a single direction.

In our experiments, colloidal particles were confined between two glass slides and subjected to a spatially asymmetric and periodic a.c. electric field E, which was successively turned on and off. The field was generated by interdigitated electrode deposited on one of the glass slides with standard photolithographic techniques (Innovations Couches Minces Co., Le Coudray Montceaux, France), the shape of which provided the necessary asymmetry (Fig. 2). The 'Christmas tree' design was chosen in such a way that the dielectric energy profile ($-\frac{1}{2}\Delta\alpha E^2$; where $\Delta\alpha$ is the polarizability of the particle relative to the suspending solution) along a line between two adjacent electrodes, was similar to that in Fig. 1, with a 50-μm period. The neck width between two adjacent electrodes was 5 μm, giving fields as high as 2×10^4 V cm^{-1} for applied voltages of just 10 V.

Experiments were performed on functionalized polystyrene latex spheres of diameter 0.25 μm, 0.4 μm (fluorescent particles provided by Molecular Probes, Eugene, Oregon) and 1 μm (provided by Interchim, Montluçon, France). The particles were suspended solution (tris (trishydroxymethyl)aminomethane) 44.5 mM, boric acid 44.5 mM, EDTA (ethylenediaminetetraacetic acid) 1.2 mM, in water), promoting substantial dissociation of the carboxylate groups at their surface. These conditions were prefered to 'pure' water both because of the easy control of the solution, and its wide use in biological systems. Electrodes were not protected by a passivation layer, and in order to avoid electrolysis a.c. voltages with frequencies higher than 500 Hz were applied. The particle diameters were measured by light-scattering techniques and found to be within 10% of the specifications; their diffusion constants were measured from direct observation of the brownian motion between glass slides, and found to agree with the Stokes–Einstein formula within 15% (diffusion close to the walls is discussed in a preprint by L. Faucheux and A. Libchaber, NEC Research Institute, Princeton NJ). Their dielectrophoretic response was also studied independently, and revealed

complex behaviour with two relaxation frequencies (J.R., unpublished results). Correspondingly, in our experiment the particles were clearly attracted into the necks of the electrode pattern for two frequency ranges, the second range depending on the size of the particle. At these frequencies, it was easy to achieve conditions such that the trapping energy was significantly larger than kT. This was simply checked by observing that the escape probability was vanishingly small.

A direct analysis of video images allowed us to count the number of particles migrating from one 'trap' to the attraction zone of the next one at each temporal on–off cycle (Fig. 3), and thus to evaluate the average induced velocity. Almost no particles were able to make backward steps. Particles of each size were studied separately at the optimal frequency defined above. Data on 20–50 different traps were accumulated, and several particle densities were investigated. The results reported here correspond to a 'low-density' regime, in that the observed diffusion process during the 'off' period was consistent with single-particle diffusion. The number of particles per trap never exceeded 20 (note however that it allowed the formation of 'strings of pearls' during the 'on' state for the 1-μm particles). Because of the time limitation imposed by the adsorption of particles on the electrodes, we proceeded in two steps for each sample. First, the border between the attraction zones of neighbouring traps was determined (Fig. 2)—its actual shape, intermediate between a circle centred on the electrode neck and a straight line perpendicular to the polar axis, shows that a complete description of the electric-field geometry requires more than a single typical length a. Second, particles were released after trapping, and their diffusion observed. We plot in Fig. 4 the fraction p of particles having crossed the above-mentioned border as a function of the 'off' time τ_{off}. We checked in the case of 0.4-μm particles that this procedure gave the same result as the counting of actual jumps during on–off cycles.

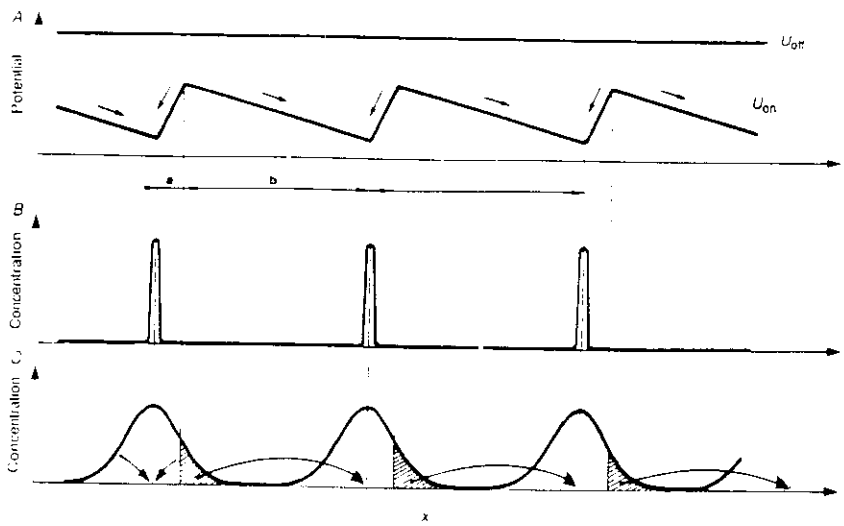

FIG. 1 Schematic illustration of the pumping principles.

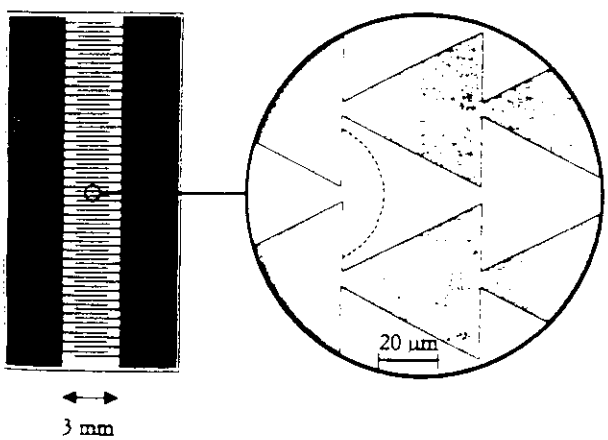

FIG. 2 *a*, Schematic representation of the interdigitated electrodes. *b*, Magnified view, and characteristics of the electrical geometry at high frequencies, as inferred from direct observation of particle motion when a voltage difference is applied between the electrodes. Particles are trapped slightly to the right of the electrode necks. The boundary (dotted line) between the attraction zones of neighbouring traps is found to be roughly circular, the minimum distance from the trap to the boundary being a.

In the simplest theoretical picture (isotropic two-dimensional diffusion) p is bounded by the probability $p_1 = 1/2 \exp(-a^2/4D\tau_{off})$ corresponding to a circular boundary and the probability $p_2 = 1/2 \operatorname{erfc}(a/(4D\tau_{off})^{1/2})$ corresponding to a straight boundary. As the diffusion constant D is measured independently and a can be estimated experimentally by direct observation, there are in principle no adjustable parameters. It is actually impossible to get $p_2 < p < p_1$ over the whole range of τ_{off} values. This could be due to many factors including non-isotropic diffusion, complex electric-field geometry that cannot be described by a single parameter a and three-dimensional effects due to the finite thickness of the sample and the presence of the electrodes. Visual observation of the process indeed suggests that particles seldom cross the neck between electrodes during the diffusion process, the result of which is that they diffuse 'forwards'. Confirmation is provided (Fig. 4) by the good fit to the data of $p \approx 0.9 \exp(-a^2/4D\tau_{off})$, the prefactor 0.9 revealing non-isotropic diffusion.

We can learn two things from these observations. First, the drift that we observe is in semiquantitative agreement with that predicted by refs 2 and 3. The values of p shown in Fig. 4 correspond to macroscopic velocities $V = pl/(\tau_{off} + \tau_{on})$, where $l \approx 50$ μm is the period of the 'Christmas tree' electrode. Plotted against τ_{off} at a fixed value of τ_{on} (~30 s was in all cases sufficient to achieve trapping), V peaks at values of the order of 0.2 μm s^{-1}.

Second, the use of this phenomenon in a separation (or selective pumping) device[5] is obvious, as the velocities depend significantly on the particle size. In fact, the selectivity is much better than suggested by Fig. 4 because for each particle size the optimum frequency has been chosen, whereas in practical circumstances one would use the same frequency for all particles. Such devices are in principle well suited for viruses, DNA molecules and complete chromosomes, because their size falls within the range investigated here. The 'Christmas tree' structure was chosen for its visual convenience, but a better design of the electrodes could also improve their performance.

Our experiment could be thought of as a simple mimic of motor protein assemblies, which have recently been given much theoretical attention[4,6,7,9,10]. It has been shown that if the motor protein evolves between at least two states in which it interacts differently with the asymmetric filament (actin or tubulin), and if the transition from one state to the other is triggered by an external agent such as adenosine triphosphate (ATP), then the motor will actively move along the filament[4]. In our experiment the electrodes provide the asymmetric

41

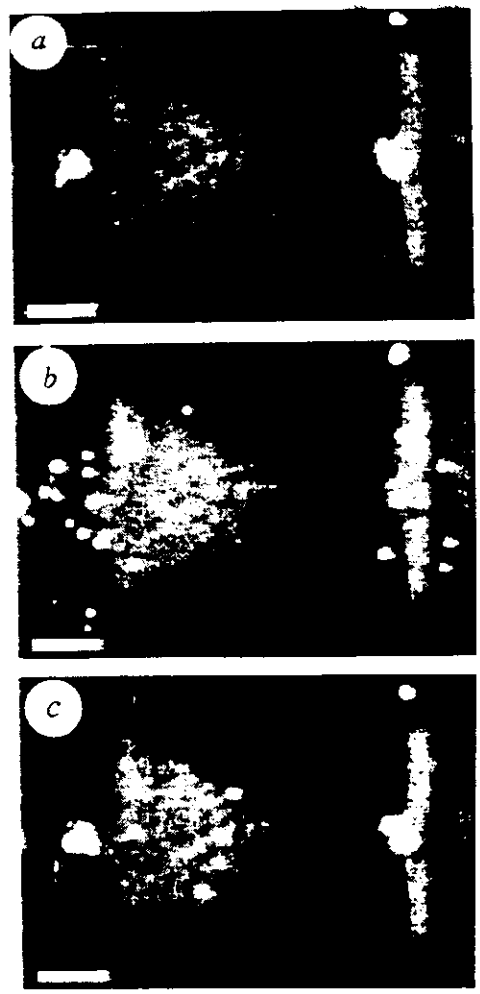

FIG. 3 Pictures of the population of colloidal particles during an on/off cycle as seen by fluorescence microscopy. Scale bar at lower left corner, 10 μm. *a*, Trapping of the 0.4-μm particles under the action of a 5 V, 500 kHz voltage. *b*, Dispersion of the particles after diffusion in the 'off' state for 24 s. *c*, Snapshot of a late stage of the retrapping process, after 18 s in the subsequent 'on' state. Most of the particles are already trapped, but in the middle of the picture are four particles on their way to the trapping site situated on the right of the picture. The sample thickness of ~3 μm (as measured either directly by focusing successively on the upper and lower boundaries of the sample, or by measuring the final diameter of a squeezed polystyrene sphere of initial diameter 15 μm) was kept small enough to prevent charge injection instabilities[12].

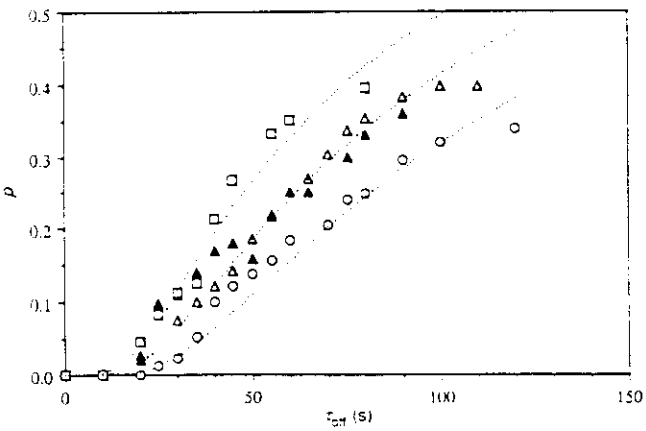

FIG. 4 Proportion p of particles diffusing from one trap to the attraction zone of the next during an 'off' (field-free) period, as a function of the time lapse τ_{off} of this period. The different plots correspond to different particle sizes and frequencies of the electric field: 0.25 μm and 800 kHz (open squares); 0.4 μm and 500 kHz (open triangles); 1.0 μm and 60 kHz (open circles). The solid triangles correspond to the direct measurement of the proportion of particles actually captured by the next trap over a cycle. The dotted lines correspond to $p \approx 0.9 \exp(-a^2/4D\tau_{off})$ with a equal to 19, 18 and 14 μm for particles of diameter 0.25, 0.4 and 1.0 μm respectively. The frequencies were chosen in such a way that the trapping occured slightly after the neck on the wide side. This favoured efficient pumping.

environment, and the 'on' and 'off' periods mimic the two states. The externally imposed regular switch between 'on' and 'off' maintains the system out of equilibrium, as the ATP does in biological systems. Note that if we scale our observed velocities with a diffusion coefficient of the order of 10^{-11} cm^2 s^{-1}, even though significantly smaller than in ref. 11, and the filament period of 8 nm (in the case of tubulin) while keeping the same asymmetry, we find optimal velocities of the order of 1 μm s^{-1} which is the same order of magnitude found for dynein tubulin systems.

Received 21 March; accepted 28 June 1994.

1. Curie, P. *J. Phys. (Paris) III* **3,** 393 (1894).
2. Ajdari, A. thesis, Univ. Paris 6 (1992).
3. Ajdari, A. & Prost, J. *C.r. acad. Séanc. Acad. Sci., Paris II* **315,** 1635–1639 (1992).
4. Prost, J., Chauwin, J.-F., Peliti, L. & Ajdari, A. *Phys. Rev. Lett.* **72,** 2652–2655 (1994).
5. Feynman, R. P., Leighton, R. B. & Sands, M. in *The Feynman Lectures on Physics* Vol. 1 Ch. 46 (Addison-Wesley, Reading, Massachusetts, 1966).
6. Astumian, R. D. & Bier, M. *Phys. Rev. Lett.* **72,** 1766–1769 (1994).
7. Peskin, C. S., Ermentrout, G. B. & Oster, G. F. in *Cell Mechanics and Cellular Engineering* (ed. Mow, V. *et al.*) (Springer, New York, 1994).
8. Ajdari, A., Lewiner, J., Prost, J. & Viovy, J.-L. French Patent No. 9311346 (1993).
9. Magnasco, M. O. *Phys. Rev. Lett.* **71,** 1477–1481 (1993).
10. Doering, C. R., Horsthemke, W. & Riordan, J. *Phys. Rev. Lett.* **72,** 2984–2987 (1994).
11. Cordova, N. J., Vale, R. D. & Oster, G. F. in *Biologically Inspired Physics* (ed. Peliti, L.) 207–215 (Plenum, New York, 1991).
12. Felici, N. *C.r. acad. Séanc. Acad. Sci., Paris, Serie B* **273,** 1004–1007 (1971).

ACKNOWLEDGEMENTS. We thank P. Barois and J.-L. Viovy for their help and advice.

2) Motor collections:

As we already mentionned muscle contraction, cell separation at the end of mitosis and many regulatory processes in living organisms, motility usually involve a large number of motors working together, and it is natural to try to understand in what way the fact of having many such motors changes the picture. The following exemple shows that in fact the situation can be dramatically different. Whereas in the one motor case the symmetry of the problem is essential it is not in the many motors one.

The reason is that in a many body problem one can have symmetry breaking. Let us consider the potentials of figure 19: W_2 is "flat" that is constant, and W_1 symmetrical. Assume now that the transition from state one to state two can only occur at the minima of $W_1(x)$.

Since motors are distributed at random (or on a lattice incommensurate with that of the actin filament), we need only to calculate the average force developped by the motors to infer what kind of motion we should expect. At very

Slow excitation rate the velocity / force relation should only involve a standard friction coefficient. Suppose however that we pull the motors (coherently around together by either the potentiometer, or the rails bumper) to the right. Those motors which are to the right of W_1 minimum are predominantly in the upper state since they have been excited ~~the other~~ while going through the minimum (and probabilities $P_2 = \omega_2^{-1}$ is well known). ~~Therefore~~ As such they contribute to very little force to the left. Those motors which are to the left of W_1 minimum, are predominantly in the ground state since they have ample time to "de excite". As such they contribute significantly to a force directed to the right. The resulting force directed to the right helps the motion, and if it overwhelms the natural friction force, spontaneous motion occurs. Note that our argument works as well with an initial velocity to the left. The spontaneous motion can occur in either direction. Now symmetry is broken spontaneously like in any phase

transition ~~metal~~ oxide is paramagnetic - ferromagnetic transitions. In fact we know that filaments are polar, the problem is now similar to that of the liquid-vapor critical point. This has consequences which, if true, would be observable: in the first order transition again it would not be possible to move continuously the voltage by applying an external force. Another remarkable consequence of the model (over 50%) is the very high efficiency, for a wide range of permittivity values $W_1(\omega)$ and $W_2(\omega)$ (not only the ones of the example). Eventually symmetry might be here like in liquid crystal displays: just to choose one of the solutions but the system might sit close to a spontaneous transition which would help having large efficiencies.

Cooperative Molecular Motors

Frank Jülicher[1,2] and Jacques Prost[1,3,4]

[1]*Institute for Theoretical Physics, University of California, Santa Barbara, California 93106*
[2]*Department of Physics, Simon Fraser University, Burnaby, British Columbia, Canada V5A 1S6*
[3]*Ecole Supérieure de Physique et de Chimie Industrielles de la Ville de Paris, 10 rue Vauquelin, 75231 Paris Cedex 05, France*
[4]*Institut Curie, 11 rue Pierre et Marie Curie, 75231 Paris Cedex 05, France*

(Received 25 April 1995)

We present a simple stochastical model for motor molecules that cooperate in large groups. This model could apply for actin-myosin motors in muscles and for motility assays with a high concentration of motor molecules. We calculate the dependence of the velocity on the applied force as a function of ATP concentration and show the existence of a dynamical phase transition allowing for spontaneous directed motion even if the system is spatially symmetric. In the symmetric case, the problem is isomorphous to a paramagnet-ferromagnet transition, in the asymmetric case to a liquid-vapor transition.

PACS numbers: 87.45.Bp, 05.40.+j, 87.10.+e

Many active processes in biological systems such as muscular contraction, cell motility, and some cellular transport processes are mediated by molecular motors. These motors are protein molecules that can perform mechanical work in the presence of adenosine triphosphate (ATP) as an energy source [1].

Different families of motor proteins have been distinguished that actively slide along rodlike filaments. These filaments play the role of a track to guide the motion. Dyneins and kinesins operate on microtubules while myosins walk along actin filaments. In many cases, these motor molecules do not operate as single particles but cooperate in groups that form a multimotor [1,2].

The most prominent example of a multimotor is the actin-myosin system in muscles [1,3]. Electron microscopy and x-ray diffraction studies of muscle fibers reveal that many myosin molecules are attached to each other with their tails and form myosin filaments. The heads of the myosin molecules are bound to actin filaments. During muscular contraction, the myosin filaments actively slide along actin filaments driven by the chemical energy of ATP. The spacing of actin monomers along the actin filaments bear no special relation with the spacing of myosin molecules in the myosin filament, so that it is a good starting point to consider the motors and track structure as incommensurate [3].

Recent improvements of experimental techniques allow the direct observation of the action of motor proteins [4–6]. In motility assay studies, a glass surface is coated with motor molecules in aqueous solution. Track filaments bound to the motors begin to move along the surface in the presence of ATP [4,6,7]. The sliding velocity can be measured as a function of ATP concentration. However, since the function of motors is not directly observable at molecular scales, the mechanisms of force generation are still not resolved.

Simplified stochastical models have been suggested that give insight in the physical mechanisms important for the force generation of molecular motors. They take into account fluctuations and Brownian motion [2,8–12]. Besides the work of Leibler and Huse [2], who compared the situations of single motors and motors working together in large groups, the previous theoretical work focused on mechanisms for the directed motion of single motor molecules [8–12].

In this Letter, we introduce a theoretical model to describe the cooperative behavior of large ensembles of motors. The motor molecules are described as particles that are attached to a backbone. The model addresses incommensurate or disordered arrangements of particles that correspond to the situations in muscle fibers and motility assays, respectively. The sliding velocity of the backbone along its track is calculated as a function of the external force and the ATP concentration.

We show that the cooperation of a large number of particles can lead to dynamical phase transitions and instabilities that characterize the behavior of such a motor collection. It turns out that cooperating motors can generate a directed force even if the system is symmetric. The direction of motion of a symmetric system is selected by spontaneous symmetry breaking.

We define our model for the most simple case, where particles are rigidly attached to a backbone with fixed spacing s. The position $\hat{x}_i$ of the ith particle reads $\hat{x}_i = is + X$, where X is the position of the backbone along its track. Each particle in the vicinity of the track can be either in a strongly bound state $\sigma = 1$ or in a weakly bound state $\sigma = 2$. The energy of a particle in state σ is given by periodic potentials $W_\sigma(\hat{x}) = W_\sigma(\hat{x} + l)$ with period l. This periodicity reflects the regular surface structure of the track filament formed by subunits of size l. From now on, we use cyclic coordinates $x \equiv \hat{x} \bmod l$ with $0 < x < l$, which describe the particle positions with respect to the potential period.

The system is characterized by distribution functions P and P_σ with $P(x,t) = P_1(x,t) + P_2(x,t)$, which give

 0031-9007/95/75(13)/2618(4)$06.00

the probability density to find a particle in state σ at position x at time t. For a finite number N of particles, $P(x,t) \equiv N^{-1}\sum_{i=1}^{N}\delta(x - x_i(t))$. We are interested in the limit of large N. In this limit, P approaches a constant value $P(x,t) = 1/l$ if the structure of motors and track is incommensurate, i.e., the ratio l/s is irrational. The same result holds if the particles are randomly attached to the backbone with a homogeneous distribution.

The equations of motion for P_σ read

$$\partial_t P_1 + v\partial_x P_1 = -\omega_1(x)P_1 + \omega_2(x)P_2, \quad (1)$$

$$\partial_t P_2 + v\partial_x P_2 = \omega_1(x)P_1 - \omega_2(x)P_2. \quad (2)$$

Here, $\omega_1(x)$ and $\omega_2(x)$ denote the transition rates between the two states. The velocity of the backbone $v \equiv \partial_t X$ is determined by the relation $f_{\rm ext} = \lambda_0 v - f$, which expresses the externally applied force per particle $f_{\rm ext}$ in terms of the force per particle

$$f \equiv -\int_0^l dx\,(P_1\,\partial_x W_1 + P_2\,\partial_x W_2), \quad (3)$$

exerted by the potentials. The friction force $\lambda_0 v$ is due to viscous damping with damping coefficient λ_0.

Transitions between the two states are (i) thermal transitions, which obey detailed balance, and (ii) ATP driven excitations, which do not obey detailed balance and which drive the active motion of the motors. We write $\omega_1(x) = \omega_2(x)\exp\{[W_1(x) - W_2(x)]/T\} + \Omega\Theta(x)$, where T denotes temperature [9]. The excitation amplitude Ω is proportional to the concentration of ATP and $\Theta(x)$ describes the x dependence of ATP excitations. For $\Omega = 0$, detailed balance is preserved.

Using the relation $P_2 = -P_1 + 1/l$, which is valid for an incommensurate or disordered system, the probability distribution in the steady state obeys

$$v\,\partial_x P_1 = -[\omega_1(x) + \omega_2(x)]P_1 + \omega_2(x)/l. \quad (4)$$

It is of pedagogical value to solve (4) in a power expansion as a function of v,

$$P_1 = \sum_{n=0}^{\infty} v^n P_1^{(n)} \quad \text{with } P_1^{(n)} = -\frac{1}{\omega_1 + \omega_2}\,\partial_x P_1^{(n-1)} \quad (5)$$

and $P_1^{(0)} = \omega_2/(\omega_1 + \omega_2)l$. The equation for v is then

$$f_{\rm ext} - f_\Omega^{(0)} = (\lambda_0 + f_\Omega^{(1)})v + \sum_{n=2}^{\infty} f_\Omega^{(n)} v^n, \quad (6)$$

with $f_\Omega^{(n)} = \int_0^l P_1^{(n)}\partial_x(W_1 - W_2)\,dx$.

If detailed balance is preserved ($\Omega = 0$, absence of ATP) $f_\Omega^{(0)} = 0$, $f_\Omega^{(1)} > 0$, there is no spontaneous motion, friction is increased. If detailed balance is broken, two important features appear: (i) $f_\Omega^{(0)}$ becomes different from zero; the system can set itself into motion spontaneously. This appearance of a self-propelling force has already been discussed in the framework of single motors [8,9]. (ii) $f_\Omega^{(1)}$ can become negative. This is a qualitatively new feature stemming from the "cooperativity" of motors. To better understand the implications of this sign change, we consider first a symmetric track filament. Under such circumstances, Eq. (6) reads to relevant order (with the condition of no external force $f_{\rm ext} = 0$),

$$-(\lambda_0 + f_\Omega^{(1)})v = v^3 f_\Omega^{(3)} + O(v^5). \quad (7)$$

If $\lambda_0 + f_\Omega^{(1)} > 0$, the only solution is $v = 0$. If $\lambda_0 + f_\Omega^{(1)} < 0$, the system bifurcates towards a moving solution [see Fig. 1(a)] with

$$v = \pm\left(\frac{1}{f_\Omega^{(3)}}\,\frac{\partial f_{(\Omega=\Omega_c)}^{(1)}}{\partial\Omega}\,(\Omega - \Omega_c)\right)^{1/2}, \quad (8)$$

where Ω_c is the critical excitation rate for which $\lambda_0 + f_{\Omega_c}^{(1)} = 0$. The solution with $v = 0$ is stable for $\Omega < \Omega_c$ and becomes unstable for $\Omega > \Omega_c$. In the latter case, starting with $v = 0$, any small perturbation grows in time because the force f exerted by the potentials acts to increase the velocity. Eventually the system reaches a state with constant velocity v as given by (8). This state is stable with respect to small perturbations. The direction of motion is selected randomly as a result of fluctuations via spontaneous symmetry breaking. With an external force, the problem is formally equivalent to that

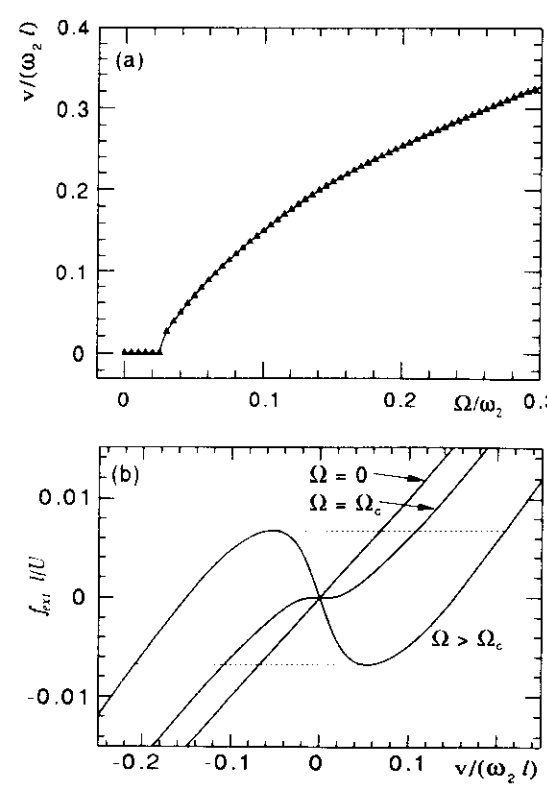

FIG. 1. (a) Spontaneous velocity v as a function of the excitation amplitude Ω for a symmetric potential as shown in Fig. 2(b) with $d/l = 0.1$ and $\lambda_0\omega_2 l^2/U = 0.1$. (b) External force $f_{\rm ext}$ as a function of the velocity v for the same system and $\Omega = 0$, $\Omega/\omega_2 = \Omega_c/\omega_2 \simeq 0.026$ and $\Omega/\omega_2 = 0.1$.

of a magnetization in the presence of a magnetic field close to a paramagnetic-ferromagnetic critical point [see Fig. 1(b)].

The general case of an asymmetric filament is now equivalent to that of a liquid-vapor critical point. The velocity corresponds to the density, the excitation amplitude to temperature, and the force to pressure. The critical point v_c, f_c, Ω_c can be defined in exactly the same way as in the case of fluids, and the velocity in its vicinity obeys the standard mean field laws $[|v - v_c| \propto (f_{ext} - f_c)^{1/3}, \Omega = \Omega_c; |v - v_c| \propto (\Omega - \Omega_c)^{1/2}, f_{ext} = f_c]$.

We postpone for a more detailed article the corresponding discussion and prefer to illustrate these considerations on a simple example. We choose a piecewise linear potential W_1, a constant W_2, and a piecewise constant rate of ATP excitations as described in Fig. 2. For simplicity, we assume that ω_2 is constant, and we look at the limit of small temperatures compared to the potential barriers $T \ll U$. In this limit, $\omega_1(x) = \Omega\Theta(x)$, and thermal excitations are neglected. The (f_{ext}, v) diagram is plotted in Fig. 3(a) for an asymmetric track filament and different values of Ω: For $\Omega < \Omega_c$, v increases monotonously as a function of f_{ext}. The effective friction coefficient $\lambda \equiv \partial f_{ext}/\partial v$ is everywhere positive. For $\Omega = \Omega_c$, v increases monotonously as a function of f_{ext} but at the critical point $\partial f_{ext}/\partial v = \partial^2 f_{ext}/\partial v^2 = 0$. For $\Omega > \Omega_c$, the function $v(f_{ext})$ is multivalued in a certain region, like a van der Waals isotherm below the critical temperature: the two steady states with $\partial f_{ext}/\partial v > 0$ are stable, the intermediate one with $\partial f_{ext}/\partial v < 0$ is unstable.

The existence of unstable steady states leads to discontinuities of v as a function of f_{ext} as follows: first, we look at the load-free velocity (i.e., $f_{ext} = 0$). If a load is applied, i.e., $f_{ext} < 0$, v decreases. The maximal load $|f_{max}|$ the collection of motors can carry is determined at the minimum of the function $f_{ext}(v)$. If this load is exceeded, i.e., $|f_{ext}| > |f_{max}|$, the system changes its direction of motion discontinuously. For reverse motion, a similar instability occurs at the maximum of $f_{ext}(v)$. These discontinuities are indicated in Fig. 3(a) for $\Omega/\omega_2 = 0.02$ by horizontal lines. This instability occurs for finite velocity. The system therefore becomes unstable before the motion is stopped: It cannot be reversed continuously by applying an external force. In an experimental situation this instability would look like a sudden "rip-off" of the track filament from the motors as soon as a critical load is reached.

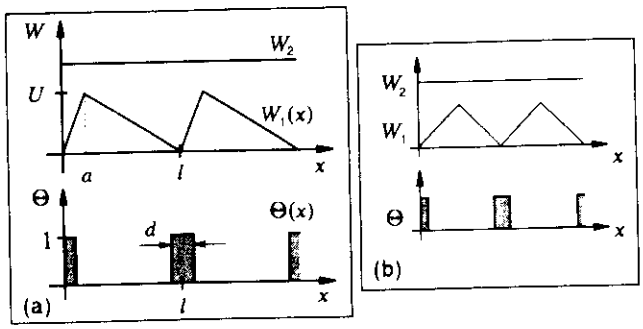

FIG. 2. Schematic diagrams of the potentials $W_1(x)$, $W_2(x)$, and the rate of ATP excitations $\Omega\Theta(x)$ for an asymmetric system (a) and a symmetric system (b). The potentials are characterized by the amplitude U, the period l, and the asymmetry parameter a/l of the sawtooth potential W_1. ATP excitations occur only within an interval of width d, centered at the potential minimum where $\Theta(x) = 1$.

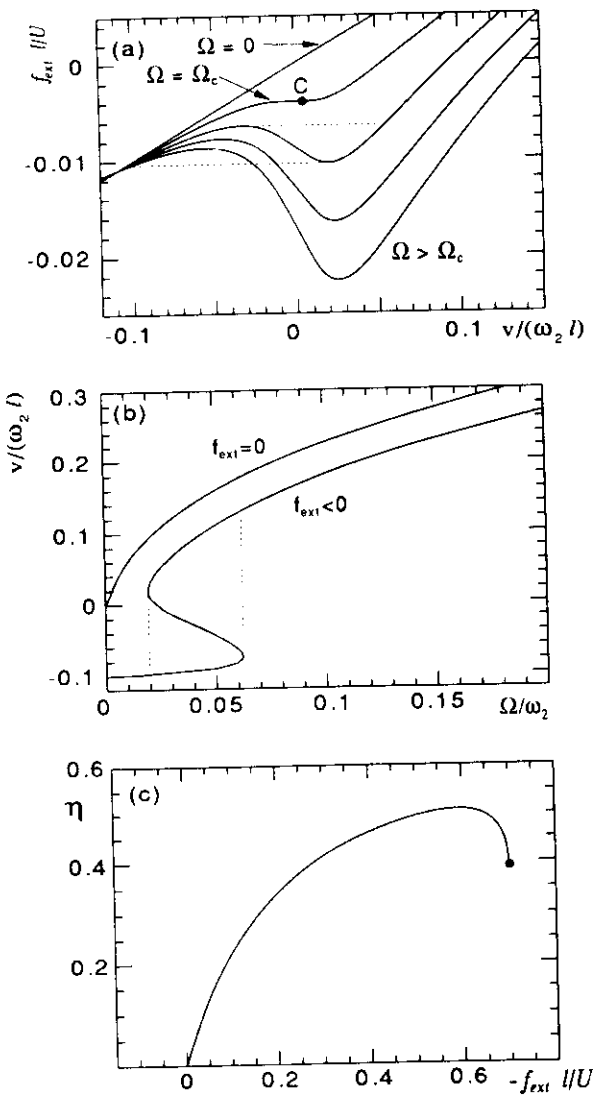

FIG. 3. (a) External force f_{ext} as a function of the velocity v for an asymmetric potential as shown in Fig. 2(a) with $d/l = a/l = 0.1$ and $\lambda_0\omega_2 l^2/U = 0.1$. The curves correspond to $\Omega/\omega_2 = 0$, 0.009, 0.02, 0.03, and 0.04, from top to bottom. Note the critical isoexcitation (equivalent to critical isotherm) for $\Omega/\omega_2 = \Omega_c/\omega_2 = 0.009$, which includes the critical point C with critical values $v_c/\omega_2 l \simeq 0.005$, $f_c l/U \simeq -0.004$. (b) Sliding velocity v as a function of Ω for $f_{ext} = 0$ (top) and $f_{ext} l/U = -0.01$ (bottom). (c) Efficiency η as a function of f_{ext} for $\Omega/\omega_2 = 10$ and $\Delta G = U$.

The velocity v for an asymmetric track filament is displayed as a function of the excitation amplitude Ω in Fig. 3(b). With no load, the motors begin to move for arbitrarily small Ω and reach for large Ω a maximal velocity $v/\omega_2 l \simeq 1.94$. With a constant load $f_{\rm ext} l/U = -0.01$, the system slides backwards for small Ω. If Ω is increased, the direction of motion changes discontinuously at $\Omega/\omega_2 \simeq 0.063$. For decreasing Ω, this instability occurs for $\Omega/\omega_2 \simeq 0.02$. The sliding velocity as a function of Ω is hysteretic.

An important property of the system is its efficiency $\eta \equiv \mathcal{W}/\mathcal{Q}$. Here, $\mathcal{W} \equiv -f_{\rm ext} l$ is the mechanical work performed during one potential period and

$$\mathcal{Q} \equiv \Omega \, \Delta G \, \frac{l}{v} \int_0^l dx \, P_1(x) \Theta(x) \tag{9}$$

is the energy consumption per particle along one potential period. The energy cost of exciting a particle to state $\sigma = 2$ is denoted by ΔG.

The efficiency η is displayed as a function of the load in Fig. 3(c). For increasing load, the efficiency reaches a maximum where $\eta \simeq 0.51$. It decreases again before the maximal load $|f_{\rm ext}| = |f_{\rm max}|$ is attained and the system becomes unstable.

In the examples, as shown in Figs. 1 and 3, thermal excitations are neglected. The critical point still exists if thermal excitations are taken into account, but its location in the $(f_{\rm ext}, v, \Omega)$ coordinate system varies with temperature.

The results discussed so far have been obtained with the assumption that the motors are rigidly coupled. This is equivalent to a mean field theory, which neglects fluctuations of the positions of individual particles. These fluctuations can be taken into account by elastically coupling the particles to the backbone via a spring with elastic modulus c. It can be shown that for sufficiently large values of c this generalized model exhibits the same qualitative behavior as the rigid model described here [13].

In summary, we have shown that a large number of particles, which are coupled together by a rigid backbone and which move in periodic potentials, can form a very efficient motor. This efficiency comes from the fact that no diffusive steps are required as a result of the cooperativity of the system. This cooperativity leads to the existence of instabilities and dynamical phase transitions. In the symmetric case, the transition is isomorphous to a paramagnet-ferromagnet transition, in the asymmetric case to a liquid-vapor transition. As a consequence, the velocity as a function of the applied load shows discontinuities and hysteretic behavior. In particular, the motion cannot be stopped or reversed continuously by increasing the load. An important result is the generation of a directed force and directed motion even if the system is symmetric. This behavior differs fundamentally from that of single particles where the spatial asymmetry of the system is essential.

The mechanisms for spontaneous symmetry breaking and directed motion that we propose here are not restricted to biological motors and ATP excitations. They could also be implemented in a physical system and driven by other types of excitation processes. If our model is relevant for biological motors, the characteristic behavior as described for asymmetric potentials should be observable in motility assay experiments with a high concentration of motor molecules.

F. J. acknowledges support by NSERC of Canada; F. J. and J. P. acknowledge NSF Grant No. PHY89-04035 and are grateful for the hospitality shown at the Institute for Theoretical Physics at Santa Barbara.

[1] B. Alberts, D. Bray, J. Lewis, M. Raff, K. Roberts, and J. D. Watson, *The Molecular Biology of the Cell* (Garland, New York, 1994).
[2] S. Leibler and D. Huse, J. Cell Biol. **121**, 1357 (1993).
[3] H. E. Huxley, Science **164**, 1365 (1969).
[4] J. A. Spudich, Nature (London) **348**, 284 (1990).
[5] K. Svoboda, C. F. Schmidt, B. J. Schnapp, and S. M. Block, Nature (London) **365**, 721 (1993).
[6] T. Q. P. Uyeda, S. J. Kron, and J. A. Spudich, J. Mol. Biol. **214**, 699 (1990); T. Q. P. Uyeda, H. M. Warrick, S. J. Kron, and J. A. Spudich, Nature (London) **352**, 307 (1991); Y. Y. Toyoshima, S. J. Kron, and J. A. Spudich, Proc. Natl. Acad. Sci. U.S.A. **87**, 7130 (1990); A. Ishijima, T. Doi, K. Sakurada, and T. Yanagida, Nature (London) **352**, 301 (1991); D. A. Winkelmann, L. Bourdieu, A. Ott, F. Kinose, and A. Libchaber (to be published).
[7] T. Duke, T. E. Holy, and S. Leibler, Phys. Rev. Lett. **74**, 330 (1995).
[8] A. Ajdari and J. Prost, C.R. Acad. Sci. Ser. 2, **t315**, 1635 (1992); see also A. Ajdari, Ph.D. thesis, Université Paris, 1992.
[9] J. Prost, J.-F. Chauwin, L. Peliti, and A. Ajdari, Phys. Rev. Lett. **72**, 2652 (1994); J.-F. Chauwin, A. Ajdari, and J. Prost, Europhys. Lett. **27**, 421 (1994).
[10] C. S. Peskin, G. B. Ermentrout, and G. Oster, in *Cell Mechanics and Cellular Engineering*, edited by V. Mow *et al.* (Springer, New York, 1994).
[11] R. D. Astumian and M. Bier, Phys. Rev. Lett. **72**, 1766 (1994).
[12] M. O. Magnasco, Phys. Rev. Lett. **71**, 1477 (1993); **72**, 2656 (1994).
[13] F. Jülicher and J. Prost (to be published). Relaxing the backbone rigidity raises deeper questions which will also be addressed.